ABSTRACT

Title of Thesis:	STABLE ISOTOPIC EVIDENCE FOR THE RISE OF OXYGEN AND REORGANIZATION OF THE SULFUR CYCLE FROM THE *ca.*2.4 Ga DUITSCHLAND FORMATION, SOUTH AFRICA
	Margaret Anne Baker, Master of Science, 2006
Thesis directed by:	Professor James Farquhar, Department of Geology

Metasedimentary rocks from the Transvaal Supergroup, South Africa, were used in a stable isotopic study to investigate the evolution of the Earth's early atmosphere and early biogeochemical cycles. Sulfur isotopic evidence indicates that the transition from an anoxic to and oxic surface environment is recorded in the Duitschland Formation. The mass-independent fractionation signal ($\Delta^{33}S$ and $\Delta^{36}S$) of Precambrian sulfide and sulfate samples diminishes from the Malmani Subgroup at the base of the study area to the top of the Duitschland Formation. Coincidental with the reduced mass-independent fractionation signal is a sizable jump in $\delta^{34}S$ and $\delta^{13}C$ fractionation related to biological activity. These data suggest that the rise of atmospheric oxygen to levels above which mass-independent fractionation in sulfur species in not effectively recorded occurred at the time of the deposition of the upper Duitschland Formation and was associated with a fundamental reorganization of the carbon and sulfur cycles.

STABLE ISOTOPIC EVIDENCE FOR THE RISE OF OXYGEN AND
REORGANIZATION OF THE SULFUR CYCLE FROM THE *ca.* 2.4 Ga
DUITSCHLAND FORMATION, SOUTH AFRICA

By

Margaret Anne Baker

Thesis submitted to the Faculty of the Graduate School of the
University of Maryland, College Park in partial fulfillment
of the requirements for the degree of
Master of Science
2006

Advisory Committee:

       Professor James Farquhar, Chair
       Professor Michael Brown
       Professor Alan J. Kaufman
       Professor Boswell Wing

Acknowledgements

Table of Contents

List of Figures

List of Tables

List of Equations

1.0 Setting the Scene

The evolution of the Earth and an understanding of the requirements to support life have been the topic of research in a range of scientific disciplines. Scientists are interested in the question of what makes Earth a habitable planet. Free water and an oxygen-rich atmosphere are key to life on this planet; however, there remain many questions about how and when these resources evolved. It has been suspected for some time that the early Earth did not have an oxygen-rich atmosphere. The rise of atmospheric oxygen is not thought to have been a gradual build over billions of years, but rather (at the minimum) a two step transition from anoxic to oxic. Models such as those suggested by Kasting (1993) argue for a stable reduced atmosphere with O_2 concentrations at the low concentrations of 10^{-12} present atmospheric levels (PAL), which were controlled by the delivery of reduced volcanic gases early in Earth's history. This anoxic environment would over time become a stable oxidized atmosphere with O_2 concentrations at the present levels of 0.2 bar.

The transition from a reduced atmosphere to an oxidized atmosphere is thought to have occurred as a step function, because once the O_2 source exceeded the reduction capacity of the volcanic gases, the O_2 abundance would increase until it was high enough to activate the sink from oxidative weathering of the continents. Kasting (1993) suggested a "three-box" model for the evolution of the Earth's oxic surface whereby the oceans are oxidized in two stages, with the deep oceans remaining reduced for some time after the atmosphere and surface oceans are oxidized. Scientists have worked to constrain the timing of the initial rise of atmospheric oxygen for more than 30 years.

Early work by Cloud (1972) and later paleosol work by Rye and Holland (1998) helped to identify geologic evidence for the rise of atmospheric oxygen during the early Proterozoic Era. Paleosols record the oxygen levels at the surface-atmosphere interface by using the relationship between oxidant availability and iron mobility. Cloud cited the presence and absence of reduced species, such as detrital uraninite (UO_2) and pyrite (FeS_2), and the presence of iron in red beds, which are clastic sedimentary strata that have oxidized iron (Fe_2O_3) coating on grains, to suggest that oxygen reached a discernible level in the Earth's atmosphere prior to *ca.*1900 million years (Ma).

Cloud (1988) continued work from paleosols to show that the solubility of iron in the oceans is dependent on O_2 concentrations. Iron is most mobile in its reduced form, and is normally precipitated in its oxidized form, so Holland inferred that red beds and banded ironstone formations in the geologic record were mobilized in a reduced environment and precipitated when they became oxidized. This work was later expanded in studies by Rye and Holland (1998) who undertook systematic studies of paleosols that supported the rise of atmospheric O_2 to levels sufficient to produce an oxidized surface environment around 2200 Ma.

Karhu and Holland (1996) argued that a ^{13}C enrichment in carbonate samples from around the world with ages from 2600 to 1600 Ma pointed to a significant disturbance in the carbon cycle coincident with the period in which previous paleosol studies indicated similar events. They argued that this enrichment could have been produced by the burial of organic carbon, which in turn would liberate a significant amount of O_2 leading to an oxidized atmosphere. More recent work by Bekker *et al.* (2001) in the Transvaal Supergroup has provided additional data connecting a ^{13}C

enrichment to the timing of the rise of an oxygen-rich atmosphere. Carbon data from the Duitschland Formation in the Transvaal Basin, South Africa, recorded ^{13}C enrichment in sedimentary marine carbonates that predates the Karhu and Holland (1996) by ~200 Ma, suggesting that a carbon burial event associated with the rise of atmospheric O_2 occurred at *ca.* 2400 Ma. These authors argue that the build up of O_2 was closely associated with biological activities, which were changing productivity stimulated by the maximum and minimum of similar aged glacial events.

In addition to carbon isotopic data, the findings of Farquhar *et al.* (2000) of mass-independent sulfur multiple isotopes in Archean rocks has added new evidence and a new tool to investigate the evolution of atmospheric O_2. Mass-independent fractionation of sulfur in the rock record is currently understood to be the product of photochemical reactions of volcanic gases in a low O_2 atmosphere (Farquhar *et al.*, 2000; Farquhar *et al.*, 2001; Pavlov & Kasting, 2002; Farquhar & Wing, 2003). The sensitivity of mass independent fractionation signals in the rock record to atmospheric oxygen concentrations is thought to present a unique geochemical signal that can be used to place better limits on the date of the rise of atmospheric O_2. Recent work by Bekker *et al.* (2004) used minor sulfur isotopes from the lower section of the Timeball Hill Formation of the Transvaal Supergroup, South Africa (just above the Duitschland Formation), to more precisely identify the timing of the timing of the rise of atmospheric. These authors argued that they did not find a mass independent fractionation signal in these samples, suggesting that the Earth's surface was oxic by 2316 ± 15 Ma.

This study focuses on samples from the underlying Duitschland Formation and also from the underlying Penge Band Ironstone Formation, the Tongwane Formation, and

the Malmani Subgroup to investigate the evolution of the carbon and sulfur isotopic changes during this key interval in Earth's evolution. This sequence predates the Timeball Hill Formation and was chosen to further constrain the timing of the rise of oxygen in the Earth's early atmosphere.

2.0 Introduction

<u>2.1 Sulfur Isotope Systematics</u>

There are four stable isotopes of sulfur with ^{32}S and ^{34}S, the two most abundant,

representing just over 99% of all sulfur, and the other 1% of sulfur is composed of the

two "minor" isotopes, ^{33}S and ^{36}S. The natural abundances of sulfur in the Vienna Cañon

Diablo Troilite (V-CDT) is 95.040% ^{32}S, 0.749% ^{33}S, 4.197% ^{34}S, and 0.015% ^{36}S (Ding

et al., 2001). Variations from these isotopic proportions in geologic materials are for the

most part caused by biological, thermodynamic, physical, and kinetic processes. Sulfur

isotopic compositions are described by comparing isotopic ratios that are normalized to

the more abundant ^{32}S and reported relative to the reference V-CDT in per mil (‰) using

δ notation:

$$\delta^{34}S = \left[\left\{ \frac{\left(^{34}S / _{32}S \right)_{sample}}{\left(^{34}S / _{32}S \right)_{V-CDT}} \right\} - 1 \right] \times 1000 \, , \qquad \text{Eq. 1}$$

$$\delta^{33}S = \left[\left\{ \frac{\left(^{33}S / _{32}S \right)_{sample}}{\left(^{33}S / _{32}S \right)_{V-CDT}} \right\} - 1 \right] \times 1000 \, , \text{ and} \qquad \text{Eq. 2}$$

$$\delta^{36}S = \left[\left\{ \frac{\left(^{36}S / _{32}S \right)_{sample}}{\left(^{36}S / _{32}S \right)_{V-CDT}} \right\} - 1 \right] \times 1000 \, . \qquad \text{Eq. 3}$$

Variations in these isotopic compositions are referred to as isotopic fractionations.

Sulfur fractionation in geologic materials occurs primarily due to mass difference of these

isotopes (*e.g.*, mass-dependent fractionation). Thus, the fractionation between ^{34}S and ^{32}S

would be approximately twice that of ^{33}S and ^{32}S, because the mass difference between

^{34}S and ^{32}S is 2 amu while the mass difference between ^{33}S and ^{32}S is only 1 amu. Fractionation factors,

$$^{3i}\alpha_{A-B} = \frac{\left(^{3i}S/_{32S}\right)_A}{\left(^{3i}S/_{32S}\right)_B},$$

<div align="right">Eq. 4</div>

are related by an exponential term (λ) that is proportional to this mass differences, *e.g.*,

$$^{33}\alpha = \left(^{34}\alpha\right)^{33\lambda},$$

<div align="right">Eq. 5</div>

$$^{36}\alpha = \left(^{34}\alpha\right)^{36\lambda}.$$

<div align="right">Eq. 6</div>

The exponent (λ) is not constant for all mass-dependent fractionation laws and under all conditions, but in general $^{33}\lambda$ varies within a few percent of 0.515 and $^{36}\lambda$ varies within a few percent of 1.9 (*e.g.*, Hulston & Thode, 1965; Farquhar & Wing, 2003). This mass dependent relationship has been used to define two reference mass fractionation arrays that are used for geologic interpretations and given by:

$$\left\{\frac{\left(^{33}S/_{32S}\right)_{array}}{\left(^{33}S/_{32S}\right)_{V-CDT}}\right\} = \left\{\frac{\left(^{34}S/_{32S}\right)_{array}}{\left(^{34}S/_{32S}\right)_{V-CDT}}\right\}^{0.515}, \text{ and}$$

<div align="right">Eq. 7</div>

$$\left\{\frac{\left(^{36}S/_{32S}\right)_{array}}{\left(^{36}S/_{32S}\right)_{V-CDT}}\right\} = \left\{\frac{\left(^{34}S/_{32S}\right)_{array}}{\left(^{34}S/_{32S}\right)_{V-CDT}}\right\}^{1.9}.$$

<div align="right">Eq. 8</div>

Sulfur from most geologic material with ages less than 2.0 Ga has sulfur isotopic compositions that fall very close to this reference mass fractionation array (RMF; Fig. 1); however, Farquhar *et al.* (2000) reported sulfur isotopic data for Archean samples that had isotopic compositions that significantly deviated from the RMF line. These deviations are reported using:
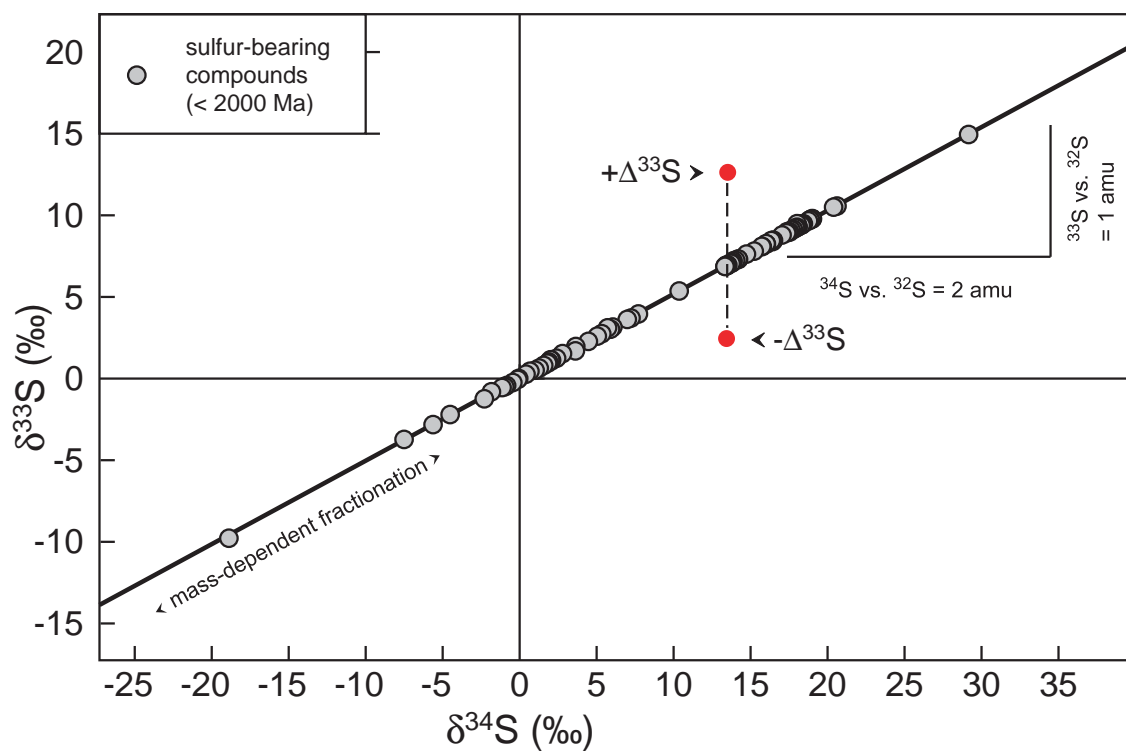
Figure 1 Reference mass fractionation (RMF) array for geologic materials younger than 2000 Ma with representative measured sulfur-multiple isotope compositions. The two red points that do not lie on the RMF are illustrative examples of mass-independent compositions. Mass-independent fractionation is indicated by a $\Delta^{33}S$ value, which is the deviation of the sample's isotopic composition from the terrestrial fractionation line. (Modified from Farquhar & Wing, 2003)

$$\Delta^{33}S = \delta^{33}S - 1000\left[\left(1 + \delta^{34}S\middle/1000\right)^{0.515} - 1\right] \text{ , and} \qquad \text{Eq. 9}$$

$$\Delta^{36}S = \delta^{36}S - 1000\left[\left(1 + \delta^{34}S\middle/1000\right)^{1.9} - 1\right]. \qquad \text{Eq. 10}$$

The large magnitude of nonzero $\Delta^{33}S$ and $\Delta^{36}S$ of Archean samples also led these authors to suggest that these deviations were produced by a group of processes referred to as mass-independent fractionation processes. Mass-independent fractionation has been shown to be the results of several processes: gas-phase photochemical reactions, nuclear reactions including cosmic ray spallation reactions, and a class of reactions referred to as hyperfine interactions (*e.g.*, Hulston & Thode, 1965; Thiemens, 1999). Hyperfine effects occur for reactions involving odd-mass isotopes as a result of coupling of spins between electrons and nuclear particles. This coupling can allow a change in the sign of the electronic spin for odd-mass isotopes and provide alternate paths for reactions that would not normally be allowed if the electron spins are not aligned. Hyperfine interactions were excluded by Farquhar *et al.* (2000) because of the correlation between the deviation of $\Delta^{33}S$ and $\Delta^{36}S$ values. If the source of the mass-independent fractionation was hyperfine interactions, then only the odd-even isotope pair (*e.g.*, $^{33}S/^{34}S$) would be affected. The possibility of nuclear effects is also ruled out on the basis of observed enrichments and depletions for both ^{33}S and ^{36}S. By process of elimination, the effect has been attributed to gas phase chemistry (*e.g.*, Farquhar *et al.*, 2000; Farquhar & Wing, 2003).

Experimental work by Bains, Sahota and Thiemens (1989), Coleman *et al.* (1996), Zmolek *et al.* (1999), Farquhar *et al.*, (2000), Farquhar *et al.* (2001) and subsequent work by Wing and others has shown that mass independent signatures of sulfur can be produced by photolysis of gaseous sulfur species. This work has shown that

large Δ^{33}S and Δ^{36}S values can be produced when reaction cells filled with SO_2 are irradiated with deep ultraviolet wavelengths. These authors suggested that the absence of oxygen and ozone in the Archean atmosphere allowed deep ultraviolet wavelengths to penetrate Earth's atmosphere and to cause photolysis of volcanogenic sulfur species to produce the mass-independent fraction record recorded in the rock record.

Figure 2 shows the evolution of Δ^{33}S values with time (Farquhar *et al.*, 2000; Farquhar *et al.*, 2001; Ono *et al.*, 2003; Mojzsis *et al.*, 2003; Hu *et al.*, 2003; Bekker *et al.*, 2004; Johnston *et al.*, 2006). The Δ^{33}S record has been used to divide Earth history into three stages that have been interpreted to reflect fundamental changes in the Earth's atmosphere and sulfur cycle (Farquhar *et al.*, 2000; Farquhar & Wing, 2003). Samples older than *ca.*2450 Ma have a large variability in Δ^{33}S values (exceeding ±1‰). Samples between *ca.*2450 and *ca.*2000 Ma have a smaller range of Δ^{33}S values (exceeding ±0.1‰), but exhibit characteristics that led Farquhar *et al.* (2001) and Farquhar and Wing (2003) to attribute a mass-independent origin. Samples younger than *ca.*2000 Ma have Δ^{33}S and δ^{34}S values that have been attributed to mass-dependent processes.
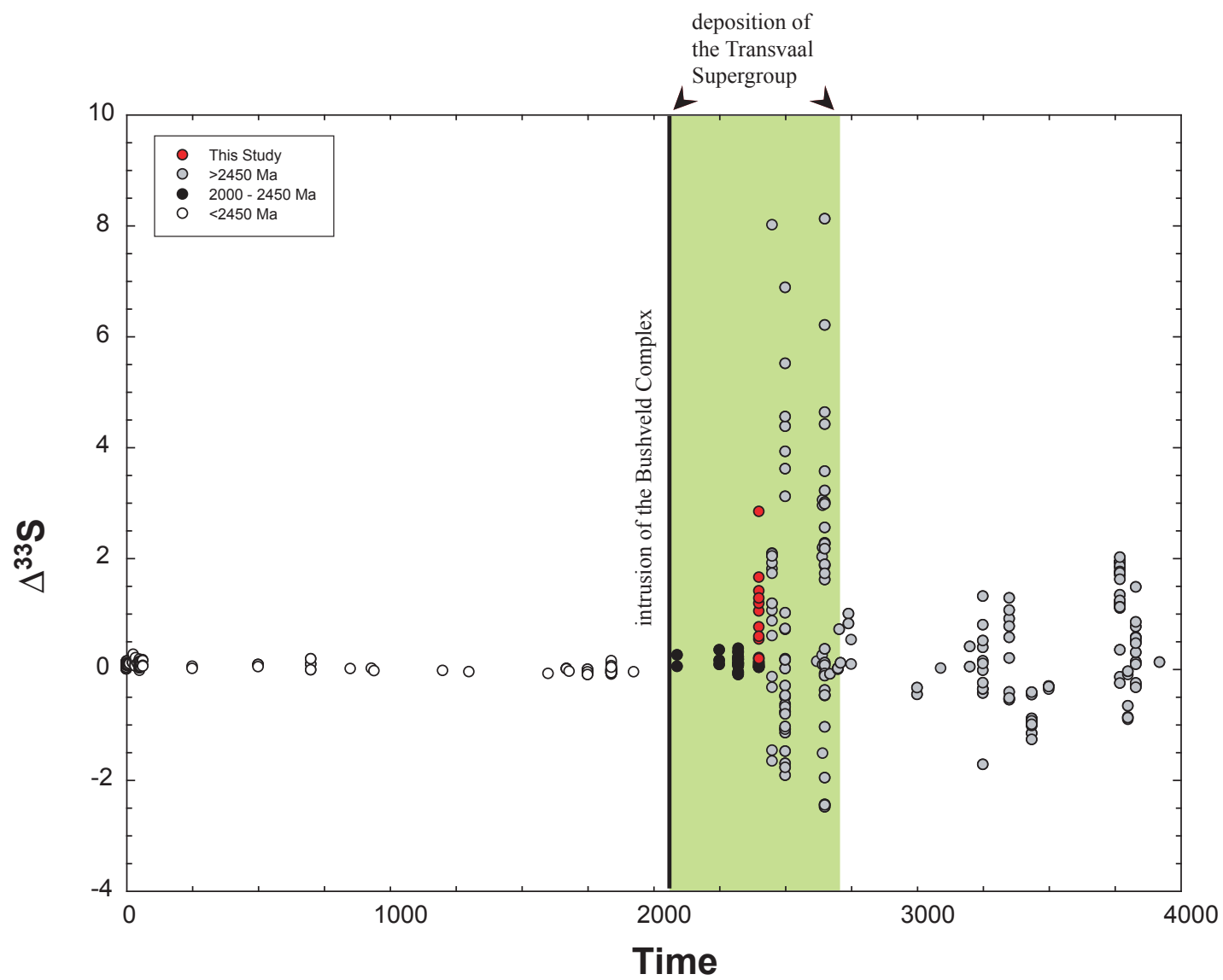
2.2 Archean Sulfur Cycle, Mass Independent Fractionation and Atmospheric Oxygen

The atmosphere of early Earth is hypothesized to have had limited free oxygen and no stratospheric ozone layer to protect the surface from ultraviolet radiation (Cloud, 1972; Holland, 1984; Rye & Holland, 1998; Pavlov & Kasting, 2002; Kasting & Catling, 2003; Catling & Claire, 2005). It has been suggested that this deep ultraviolet radiation could interact with sulfur compounds released by volcanoes to produce sulfur species (organic sulfur and sulfate) with non-mass dependent signatures that were then transferred to the surface and then preserved in the rock record. Under the current oxygen-rich atmosphere, volcanic sulfur dioxide that reaches the stratosphere may undergo photolysis and be fractionated, but the mass independent signal in various sulfur species would also be rehomogenized by the oxidation of elemental sulfur to sulfate and the transfer of this sulfur to surface reservoirs (Farquhar *et al.*, 2000; Farquhar *et al.*, 2001, Pavlov & Kasting, 2002; Farquhar & Wing, 2003). An Archean atmosphere with limited free oxygen would permit both oxidized and reduced sulfur species (Fig. 3) from volcanic gases (*e.g.*, H_2S and SO_2) to interact with solar radiation to produce both elemental sulfur aerosols (*e.g.*, S_8) and oxidized sulfur aerosols (*e.g.*, H_2SO_4). Reduced and neutral sulfur species are inferred to have been deposited in the sedimentary record providing a source of positive $\Delta^{33}S$ sulfur, and oxidized sulfur species are thought to have been deposited to the surface reservoirs, providing a source of negative $\Delta^{33}S$ sulfate sulfur (Farquhar *et al.*, 2001; Pavlov & Kasting, 2002). Pavlov and Kasting have used a

---

Figure 2   A plot of $\Delta^{33}S$ versus time compiled from Farquhar *et al.*, 2000, 2002; Ono *et al.*, 2003, 2006; Mojzsis *et al.*, 2003; Hu *et al.*, 2003; Johnston *et al.*, 2005. The different color circles are used to indicate the age range of the samples after Farquhar & Wing, 2003, which is discussed in the text. Data from Bekker *et al.*, 2004, are shown in blue from the overlying Timeball Hill Formation. Data from this study are shown in red. Also shown is the age of the intrusion of the Bushveld Complex and the time span of the deposition of the Transvaal Supergroup.

11
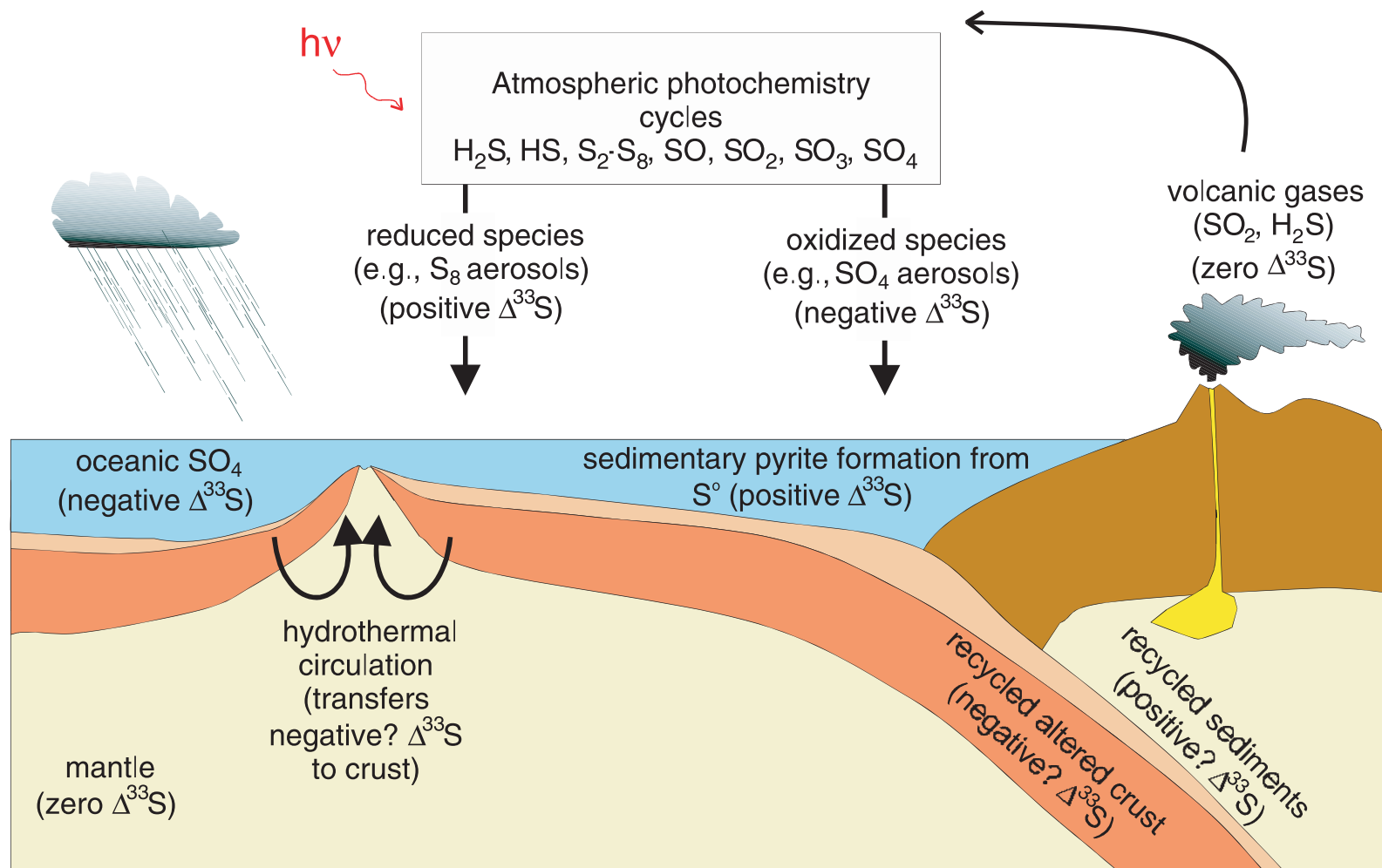
Figure 3 Diagram of the Archean sulfur cycle with corresponding $\Delta^{33}S$ values for different reservoirs and indicating the different pathways of transporting both a reduced and an oxidized sulfur signature to the surface of the Earth. From Farquhar *et al.*, 2002.

one-dimensional model of atmospheric chemistry to argue that the efficient transfer of the

atmospheric signal to the sedimentary records requires at least two pathways to preserve

the positive and negative $\Delta^{33}S$ values observed in rocks, and that an atmosphere with

more than 10^{-5} present atmospheric level (PAL) O_2 leads to most sulfur exiting the

atmosphere as sulfate. Their model results suggest the occurrence of a number of

different sulfur species in low oxygen atmosphere, and they argue that, along with any

anomalous isotopic signals, they can be transferred to the sedimentary rock record in

significant amounts. At higher concentration of atmospheric O_2, the transfer of sulfur as

sulfate overwhelms the other available pathways, reducing the sulfur mass-independent

fractionated signal in the rock record.

2.3 Carbon Isotope Systematics and Carbon Cycle

Carbon has two stable isotopes, ^{12}C and ^{13}C, that have abundances of 98.8944%

and 1.11056%, respectively (Rollinson, 1993; Coplen *et al.*, 2002). Isotopic data is

reported as delta values in per mil (‰) notation and is commonly normalized to the

Vienna PeeDee Belemnite (V-PDB) for carbonate samples.

$$\delta^{13}C = \left[\left\{ \frac{\left(^{13}C/_{12}C \right)_{sample}}{\left(^{13}C/_{12}C \right)_{V-PDB}} \right\} - 1 \right] \times 1000 \qquad \text{Eq. 11}$$

Carbon is preserved in the geologic record as both reduced organic carbon (C_{org}) and

oxidized carbonate carbon (C_{carb}) and can provide information on biological activity and

elemental cycling between the atmosphere and oceans. Carbon initially comes from

mantle sources and has a $\delta^{13}C$ of ~7‰. Organic carbon typically has negative $\delta^{13}C$

values due to the preferential incorporation of ^{12}C relative to ^{13}C in biological processes; whereas, marine carbonates typically have near zero or positive $\delta^{13}C$ values, because removal of ^{12}C-enriched carbon to the reduced reservoir leaves residual oceanic carbonate carbon reservoir that is enriched in ^{13}C.

The isotopic composition of carbon in the atmosphere-ocean system is determined by the difference between the input of carbon from volcanic and metamorphic processes ($f_{volc}\delta^{13}C_{volc}$) as well as carbon from surface weathering ($f_w\delta^{13}C_w$) and the burial of reduced carbon ($f_{org}\delta^{13}C_{org}$) and oxidized carbon ($f_{carb}\delta^{13}C_{carb}$: Kump & Arthur, 1999; Hayes *et al.*, 1999; Des Marais, 2001; Catling & Claire, 2005). Over time scales of *ca.*100 million years (My), this relationship between inputs and outputs in the atmosphere-ocean system reach a steady state:

$$f_{volc}\delta^{13}C_{volc} + f_w\delta^{13}C_w = f_{org}\delta^{13}C_{org} + f_{carb}\delta^{13}C_{carb} \ . \qquad \text{Eq. 12}$$

The right side of equation 12 can be used to discuss the isotopic composition of carbon in the sedimentary rock record based on the isotopic composition of the atmosphere-ocean system from which it was deposited, where *f* represents the fraction of carbon buried as either the reduced or oxidized species:

$$\delta^{13}C_{atmosphere-ocean} = f_{org}\delta^{13}C_{org} + f_{carb}\delta^{13}C_{carb}. \qquad \text{Eq. 13}$$

Changes in the global carbon budget over geologic time are linked to volcanic activity, biological activity, rates of carbon burial, and changes in other biogeochemical cycles such as oxygen, phosphate, and sulfur (Hayes *et al.*, 1999; Kump & Arthur, 1999; Des Marais, 2001; Ripperdan, 2001; Catling & Claire, 2005).

The modern biogeochemical carbon cycle is dominated on the short timescales (*ca.*1000 years) by the hydrosphere, atmosphere and biosphere subcycle that cycles CO_2

from the atmosphere and oceans through primarily biological fixation as organic matter that then is re-released into the atmosphere and oceans as biologic matter decomposes (Des Marais, 2001). In the longer timescale (*ca.*1000 years – 100 My) the burial and decomposition of sedimentary organic matter and marine carbonates influence the hydrosphere, atmosphere and biosphere subcycles. Other influences on the carbon cycle with a longer timescale include subduction of sedimentary and igneous carbon at convergent margins that impact the carbon cycle on a timescale of *ca.*1 – 1000 My, and the carbon reservoir of the mantle, which has a cycling time scale in the modern carbon cycle of *ca.*10 – 1000 My (Des Marais, 2001).

Figure 4 shows the $\delta^{13}C_{carb}$ values of carbonates ranging in age from 2600 to 1600 Ma compiled by Karhu and Holland (1996). These data indicate a major disturbance in the carbon cycle during the period (2200 to 2000 Ma) in which other proxies for atmospheric oxygen (*e.g.* minor sulfur isotopes and paleosols) indicate a large change in the Earth's biogeochemical cycles. Karhu and Holland (1996) note that from 2600 to 2300 Ma there is a minor depletion of $^{13}C_{carb}$ values, and at *ca.*2200 Ma, the $\delta^{13}C_{carb}$ record shows a significant enrichment of ~10‰ that lasted for *ca.*100 Ma before returning to values similar to those before the excursion. The authors suggest that this large enrichment in $^{13}C_{carb}$ values could have been produced by the enhanced proportional burial of organic carbon, producing a more enriched reservoir from which carbonate carbon is obtained that would record the more positive $\delta^{13}C_{carb}$ values. Organic carbon, however, does not record the same well defined enrichment excursion. Several other changes either in carbon input, such as increased volcanic activity, or changes in nutrients in the water column available to organisms, such as increased phosphate from continental
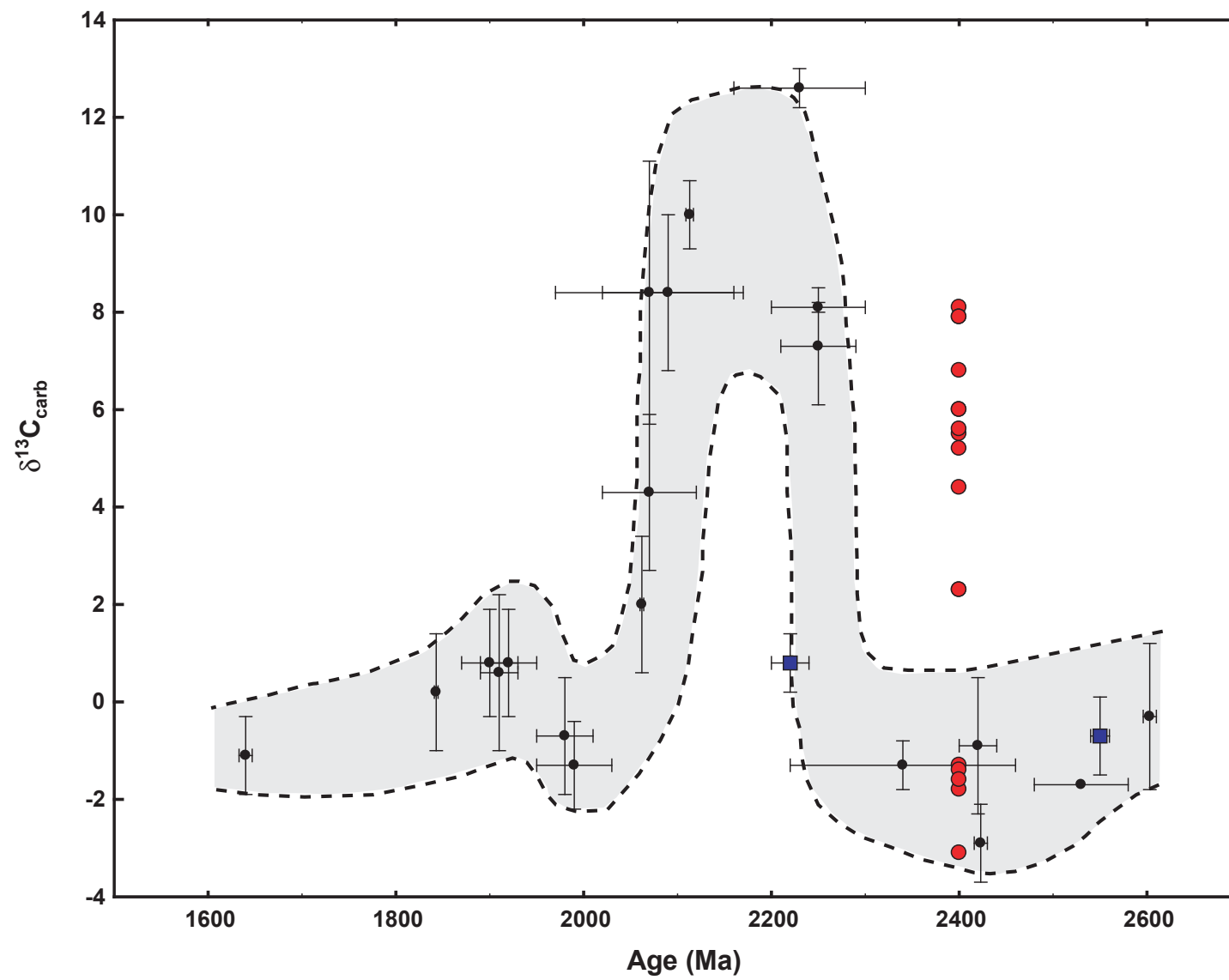
weathering and increased nutrient turnover in the oceans, can influence the isotopic fractionation between C_{org} and C_{carb} (Kump & Arthur, 1999; Hayes *et al.*, 1999; Catling *et al.*, 2005; Melezhik *et al.*, 2005; Aharon, 2005).

Karhu and Holland (1996) suggest a direct connection between a massive burial of organic carbon and the timing of the rise of atmospheric oxygen on the basis of an inferred connection between buried organic material and the release of oxygen (*e.g.*, CO_2 + $H_2O \leftrightarrow CH_2O + O_2$). According to their estimate, the ca. 100 My carbonate excursion would represent approximately 12-22 times present atmospheric levels (Karhu & Holland, 1996). This elevated level, however, would have been short lived as the O_2 was scavenged by redox-sensitive compounds in the shallow oceans and by organisms (Kasting, 1993; Canfield, 2005; Catling & Claire, 2005; Aharon, 2005).

Bekker *et al.* (2001) provided a carbon isotopic study of the *ca.* 2.4 Ga Duitschland Formation, which lies stratigraphically below the Timeball Hill Formation. These authors pointed to a $^{13}C_{carb}$ enrichment in the upper Duitschland Formation that proceeded to the glacial event recorded in the Timeball Hill Formation dated around 2316 ± 15 Ma (Bekker *et al.*, 2004; Hannah *et al.*, 2004). This carbon enrichment is *ca.*200 Ma before the $^{13}C_{carb}$ enrichment that Karhu and Holland (1996) argue is intimately connected to the rise of atmospheric O_2. Regardless of the cause of the enrichment of $\delta^{13}C_{carb}$ values, the timing of this event is concurrent with other proxies for the rise of atmospheric O_2 and with the deposition of the Pretoria Group within the Transvaal Basin that is the focus on this study.

Figure 4   Modified diagram from Karhu and Holland (1996) showing global carbonate carbon excursion. Shown in red are the data from Bekker *et al.* (2001) that pushes the carbon excursion to *ca.*200 Ma prior to the Karhu and Holland event. Samples from the Transvaal Supergroup are shown in blue.

2.4 Rise of Atmospheric Oxygen

　　Several lines of evidence point to a significant rise of atmospheric oxygen in the

interval 1900 – 2400 Ma, but there remain many questions about the cause and rate of

this rise (Cloud, 1972; Rye & Holland, 1998; Kasting, 1993; Farquhar *et al.*, 2000;

Catling *et al.*, 2001; Pavlov & Kasting, 2002; Kasting & Catling, 2003; Canfield, 2005;

Catling & Claire, 2005). The transition from an anoxic environment to an oxic

environment that sustains complex life is fundamentally a result of the rise of free

atmospheric O_2. Evidence from geochemical data and paleoenvironmental proxies

suggest that the rise of atmospheric O_2 to the present level was a two-step process that

began in the Paleoproterozoic, with the second step occurring during the Neoproterozoic.

The first phase of the oxidation of the Earth's surface changed the environment from an

anoxic atmosphere to an oxic atmosphere. In an anoxic environment the oxygenation

parameter (K_{oxy}) is less than 1 and is defined as

$$K_{oxy} = \frac{F_{source}}{F_{metamorphic} + F_{volcanic}},$$
Eq. 14

where F_{source} is the amount of photosynthetic O_2 released to the atmosphere by the burial

of reduced compounds, particularly organic matter and pyrite, and the abiotic production

due to hydrogen escape, and $F_{metamorphic}$ and $F_{volcanic}$ are the amount of O_2 used to oxidize

reduced species from these processes (Catling & Claire, 2005). The metamorphic and

volcanic sinks for O_2 are mostly reducing gases such as H_2S, H_2, CO, and SO_2. On the

modern Earth, the major source of free oxygen is oxygenic photosynthesis (*e.g.*, CO_2 +

$H_2O \rightarrow CH_2O + O_2$); however, this mechanism for O_2 requires complex biological

activity that had not developed in the early Earth.

Prior to the evolution of oxygenic photosynthesis, there was limited free oxygen due to abiotic processes. Other processes that might have increased the levels of atmospheric O_2 include hydrogen escape (ϕ_{escape}) by diffusion through the homopause (Walker, 1977; Catling *et al.*, 2001; Kasting & Catling, 2003; Catling & Kasting, 2005; Tian *et al.*, 2005; Kasting, 2005). The rate of hydrogen escape is proportional to the sum of the mixing ratios of all the hydrogen-bearing species in the atmosphere (f_{total}), above the troposphere, weighted by the number of hydrogen atoms that they contain (Walker, 1977; Kasting & Catling, 2003; Catling & Claire, 2005; Kasting, 2005). Together with a coefficient for the diffusion of hydrogen over the height of the atmosphere, hydrogen escape can be expressed as $\phi_{escape} \cong 2.5 \text{ x } 10^{13} f_{total}$ (H atoms cm^{-2} s^{-1}). According to calculations by Kasting and Catling (2003) the hydrogen escape rate for a methane-rich, pre-biota atmosphere would produce ~$2.1 \text{ x } 10^{10}$ mol O_2/year at the high end – compare this abiotic production to the biotic production of ~$1.8 \text{ x } 10^{12}$ mol O_2/year. The small amount of free oxygen would be quickly used to oxidize the reduced gas species being produced by volcanic and metamorphic activities. This production of oxygen would be too small alone to counterbalance the build up of reduced species in an anoxic atmosphere; therefore, the first step in the transition to an oxic environment could not be due to the build up of O_2 from hydrogen escape alone. Hydrogen escape could have played a key role in the transition coupled with either an increase in the production of O_2 by biological activity or the reduction of sinks for free oxygen (Catling & Claire, 2005). This initial rise in oxygen most likely coincides with fundamental changes in the Earth's environment and the evolution of eukaryotes and photosynthesis (Cloud, 1972; Rye & Holland, 1998; Kasting, 1993; Catling *et al.*, 2001; Nisbet & Sleep, 2001; Pavlov &

Kasting, 2002; Kasting & Catling, 2003; Kerr, 2005; Canfield, 2005; Catling & Claire, 2005).

Based on the carbonate record discussed above, Karhu and Holland (1996) suggested a direct connection between a massive burial of organic carbon and the timing of the Paleoproterozoic rise of atmospheric oxygen. Aharon (2005) notes that the Paleoproterozoic burial of carbon corresponds to between 6.7 x 10^{22} to 8.5 x 10^{22} g C that would produce between 18 x 10^{22} to 22 x 10^{22} g O_2, a level that would be equivalent to the entire modern O_2 concentration for the Earth's surface in one pulse. Not only is this a massive amount of O_2 to produce at one time, it would need to be reconciled with the biogeochemical data indicating that the Earth's oceans remained anoxic until the second oxidation event in the Neoproterozoic (*e.g.* Cloud, 1972; Walker, 1977; Kasting, 1993; Catling & Claire, 2005).

Kasting (2001) notes that there is wide-spread agreement that the O_2 for the Paleoproterozoic rise is closely related to the evolution of cyanobacteria. These organisms are ancient prokaryotes that use oxygenic photosynthetic pathways. Biogeochemical evidence suggest that cyanobacteria had developed the capabilities for oxygenic photosynthesis by 2700 Ma (Kasting, 2001; Catling *et al.*, 2001; Nisbet & Sleep, 2001; Kerr, 2005; Canfield, 2005; Catling & Claire, 2005). The timing of the emergence of cyanobacteria is *ca.*300 Ma before the Paleoproterozoic atmospheric oxidation event, based on the Bekker *et al.* (2001) timing for the Duitschland Formation $\delta^{13}C_{carb}$ enrichment. This lag between the emergence of photosynthetic cyanobacteria and the rise of atmospheric oxygen, however, has not quieted those who see the oxidation event as closely linked to the Paleoproterozoic pulse of organic burial as called for in the

recorded $\delta^{13}C_{carb}$ enrichment. While the change in carbonate isotopic composition and the rise of atmospheric oxygen are likely connected, this relationship is not a straight-forward cause and effect.

Instead of a single pulse of O_2 production, the $\delta^{13}C$ enriched carbonates may record a long-term increase in the burial of organic carbon and the build-up of oxygen that is coupled with a decrease in the sinks for free O_2 (Bekker *et al.*, 2001; Catling *et al.*, 2001; Kasting, 2001; Catling & Kasting, 2003; Catling & Claire, 2005). A change in the proportion of reducing gases released by volcanic and metamorphic processes could lead to an increase in hydrogen-bearing species, and therefore f_{total}, that would enhance the rate of hydrogen escape, leading to excess atmospheric oxygen (Catling *et al.*, 2001; Kasting, 2001; Catling & Claire, 2005). This mechanism could serve as the key source of oxygen and would decrease the sink of free O_2 until biologically produced oxygen overwhelmed this source and lead to the transition to an anoxic surface environment (Catling *et al.*, 2001; Catling & Claire, 2005).

2.5 Geologic Setting

The Transvaal Supergroup, located in northern South Africa, is a Neoarchean – Paleoproterozoic succession that is well preserved in the Transvaal and Griqualand West basins on the Kaapvaal craton (Eriksson *et al.*, 1993; Eriksson *et al.*, 2001). The stratigraphy of these two basins is well correlated on the basis of chronostratigraphic data from marker beds (Nelson *et al.*, 1999; Bekker *et al.*, 2001; Coetzee, 2001; Sumner & Grotzinger, 2004). Figure 5 provides a map of the Transvaal Basin sequence that is made

up of two groups: the Chuniespoort Group and the Pretoria Group. The Chuniespoort

Group is made up of primarily chemical sedimentary rocks while the overlying Pretoria

Group consists primarily of clastic sedimentary rocks (Coetzee, 2001; Eriksson *et al.*,

2001). These rocks form the basement for the intrusion of the Bushveld Igneous

Complex and in places have undergone contact metamorphism and deformation.

This study focuses on the transition from the Chuniespoort Group to the Pretoria Group,

with a concentration on the Duitschland Formation that forms the basal contact with the

Chuniespoort Group. The study area (Fig. 5) is located southwest of Mokopane (formally

Potgietersrus), South Africa, on Duitschland Farm 95 KS, and is the type locality for the

Duitschland Formation. Whereas the Duitschland Formation is the focus of this study,

samples from the Malmani Subgroup and the Penge BIF, which were collected from

outcrops on Duitschland Farm 95 KS, as well as a sample from the Tongwane Formation,

which was collected northeast of the Duitschland Farm in the Tongwane riverbed, were

also studied. Figure 6 provides a schematic section of the Transvaal Basin sequence and

published age constraints on formations surrounding the Duitschland Formation.

The base of the Chuniespoort Group is marked by the Black Reef Quartzite that is

overlain by the Malmani Subgroup, a sequence of dolomite with intercalated shale and

chert layers. The Malmani Subgroup is subdivided into five formations – Oaktree

Formation, Monte Christo Formation, Lyttelton Formation, Eccles Formation, and Frisco

Formation – based primarily on stromatolite types and minor interbedded chert and

mudstone layers (Eriksson *et al.*, 1993; Eriksson & Altermann, 1998; Eriksson *et al.*,

2001). Martin *et al.* (1999) report a SHRIMP U-Pb zircon age from the lower-most
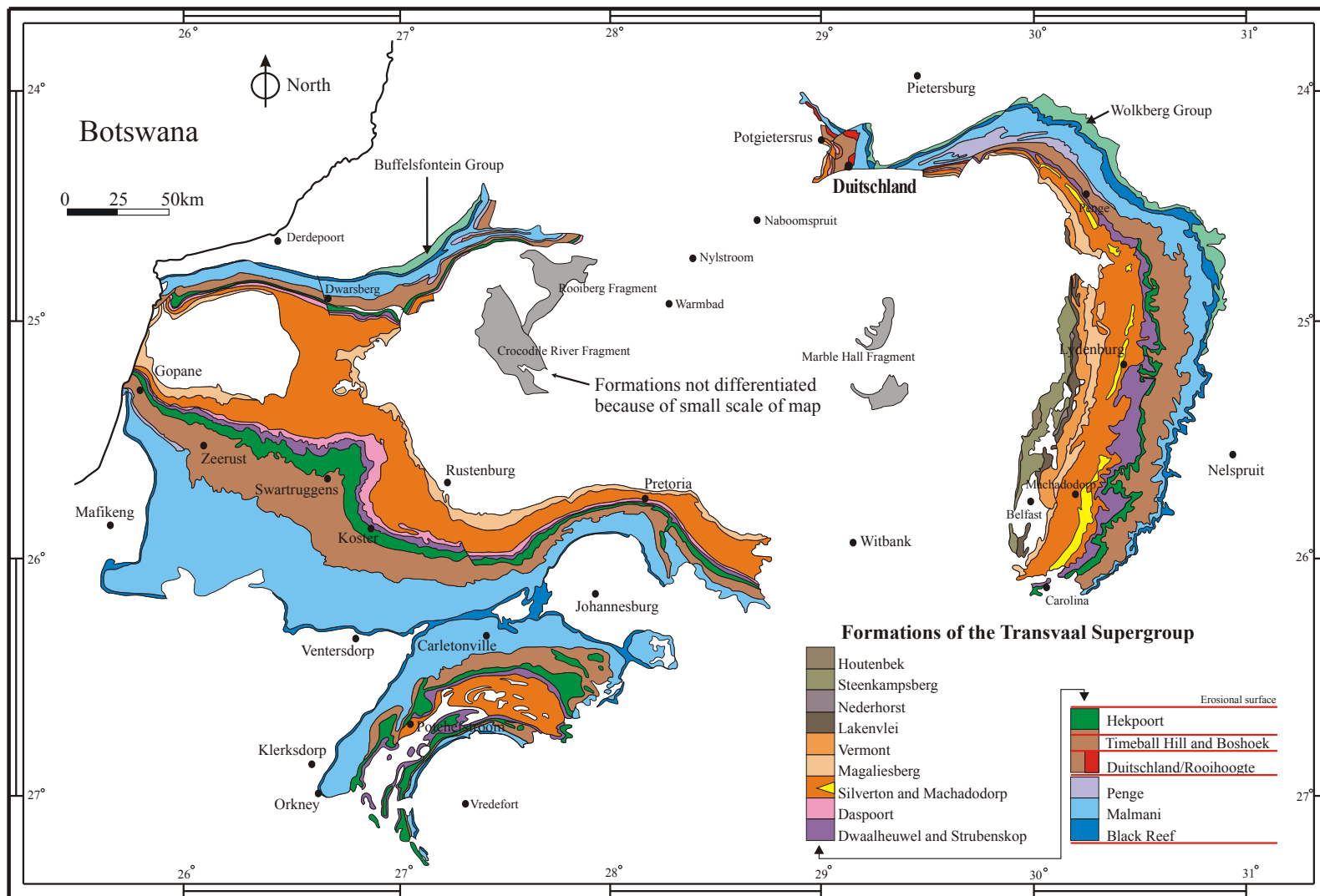
Figure 5 Geologic map of the Transvaal Basin, which is comprised of the the Chuniespoort Group and the Pretoria Group. Modified from Coetzee, 2001.

Oaktree Formation to be 2583±5 Ma (as reported in Nelson *et al.*, 1999; Bekker *et al.*, 2001).   The upper Frisco Formation has a gradational contact with the overlying Penge Banded Ironstone Formation (BIF) that is preserved in the northern section of the basin. In other sections of the Transvaal Basin, the overlying Pretoria Group has a basal cherty layer in unconformable contact with the Malmani Subgroup (Coetzee, 2001). A SHRIMP U-Pb zircon age for the Penge BIF was reported by Nelson *et al.* (1999) to be 2480±6 Ma. In the northern section of the Transvaal Basin, the Penge BIF is in conformable contact with the Tongwane Formation, an iron-rich laminated dolomite, that is not preserved in other sections of the basin (Bekker *et al.*, 2001).

The Duitschland Formation serves as the basal unit of the Pretoria Group (Nelson *et al.*, 1999; Bekker *et al.*, 2001; Coetzee, 2001; Bekker *et al.*, 2004). On Duitschland Farm, the Duitschland Formation is in unconformable contact with the underlying Penge BIF (Eriksson *et al.*, 1993; Eriksson *et al.*, 2001; Bekker *et al.*, 2001; Coetzee, 2001). This unconformity is due to the glacial erosion of the formation post the deposition of the Tongwane Formation that is not well preserved in the study area. At Duitschland Farm the Duitschland Formation has a thickness of ~1000 m and can be divided into a lower and upper section based on a sharp erosional contact that is overlain by two conglomeratic quartzite layers (Coetzee, 2001; Bekker *et al.*, 2001). This erosional surface marks a sequence boundary separating two distinct regressive sequences at ~400 m (Bekker *et al.*, 2001).   The base of the Duitschland Formation is marked by a glacial diamictite overlain by pyrite-bearing carbonaceous shales (Bekker *et al.*, 2001; Eriksson *et al.*, 2001; Coetzee, 2001). Overlying these shales are finely-laminated marly

Transvaal Basin		
Hiatus	Pretoria Group	Transvaal Supergroup
Hekpoort Formation		
Boshoek and Upper Timeball Hill Formation		
Lower Timeball Hill Formation *Re-Os pyrite age 2316 ± 7 Ma* Rooihoogte/Duitschland Formation		
Hiatus	Chuniespoort Group	
Tongwane Formation		
Penge BIF *SHIRMP U-Pb zircon age 2480 ± 6 Ma*		
Malmani Subgroup *SHRIMP U-Pb zircon ages 2583 ± 5 Ma & 2588 ± 7 Ma*		
Black Reef Quartzite		

Figure 6   Schematic representation of the Transvaal Supergroup in the Transvaal Basin with representative ages of formations surrounding the Duitschland Formation. Modified from Bekker *et al.*, 2004. The Re-Os age for the Lower Timeball Hill Formation is from Hannah *et al.*, 2004, and references within. The SHRIMP U-Pb zircon ages for the Penge BIF is from Nelson *et al.*, 1999, and for the Malmani Subgroup is from Martin *et al.*, 1998.

mudrocks. The upper portion of the formation includes a second conglomerate and is dominated by quartzite and dolomite.

This succession records an upward-shallowing paleo-environment of a shoreline regression (Eriksson *et al.*, 2001; Bekker *et al.*, 2001). Coetzee (2001) suggests that the geometry of the Duitschland Formation over the Transvaal Basin is in agreement with a foreland basin environment, with the area around Duitschland Farm being a proximal foreland trough. The Timeball Hill Formation is in unconformable contact with the Duitschland Formation. It is a glacial influenced succession with the base of the formation made up of carbonaceous shales with disseminated pyrite grains (Eriksson *et al.*, 2001; Bekker *et al.*, 2004). Hannah *et al.* (2004) provided a Re-Os age based on the analysis pyrite grains from this formation as 2316±7 Ma.

3.0 Analytical Methods

Whole rock powders were prepared for outcrop samples collected by Dr. Boswell
Wing from the study area of Duitschland Farm, ~20 km southeast of Mokopane
(Potgietersrus) South Africa, in summer 2003. Sulfur isotope work was undertaken for
each of the samples in the sample set (n=30). Carbon and oxygen isotope analyses were
undertaken for eighteen carbonate samples. Sulfur extraction from the rock powders was
accomplished by using two different extraction techniques that depended on primary
lithology and the sulfur species of interest in the samples. Samples containing carbonate-
associated sulfate (CAS) were processed by combining elements of methods described in
Thode *et al.* (1961), Burdett *et al.* (1989), and Forrest and Newman (1977). Samples
containing visible pyrite grains in shales were processed using a modified version of the
method reported in Hsieh and Shieh (1997). Rock powder from micro-drilling was used
for carbon and oxygen isotopic analyses. All analytical work was done at the University
of Maryland Stable Isotope Laboratory.

3.1.0 Sulfur Isotopic Analysis

3.1.1 Carbonate-Associated Sulfate Extraction

Carbonate-associated sulfate (CAS) was extracted from carbonate rocks by a
multistep procedure that combines elements of techniques reported in Thode *et al.*
(1961), Burdett *et al.* (1989), and Forrest and Newman (1977). Carbonate samples from
the lower section of the Duitschland Formation and from the Malmani Subgroup required
the use of ~200 gram (g) of powdered rock for adequate amount of sulfur for analysis;

whereas, samples from the upper Duitschland Formation required ~50 g. The powdered samples were first put through a series of washes to remove soluble sulfate species; ~25 – 250 g of powdered sample was placed in a beaker in which ~25 – 250 ml of 5.25% (w/w) NaOCl was added and left for at least 48 hours. The NaOCl solution was removed by vacuum filter, using a Whatman No. 1 filter. The residual solids were transferred into a beaker and placed in a Millipore water wash for at least 48 hours. The wash water was removed by filtering the sample through a Whatman No. 1 filter and discarded. In samples that used less than 50 g of rock powder, the residual solids were reacted with 3 N hydrochloric acid (HCl) to completion in a porcelain Buchner filter funnel on top of a clean Erlenmeyer flask to collect the filtrate. In samples that used more than 50 g of rock powder, the residual solids were placed into a clean 1 L plastic beaker and reacted with ~2 L of 3N HCl that was added in increments of ~150 ml every 20-30 minutes until the sample were reacted to completion. The residue was removed from these larger samples by filtration through a Whatman No. 1 filter in a porcelain Buchner filter funnel on top of a clean Erlyenmeyer flask to collect the filtrate. The filtrate was then passed through a 0.22 μm cellulose membrane filter (Millipore e02wp02500) under a vacuum to remove any fine-grained solids. The acidic filtrate solution was collected in a clean beaker and placed on a warming plate inside a closed plastic box that was flushed through HEPA filters with room air. Tests undertaken with water-filled beakers indicated that the temperature of the solutions was ~80°C, which limits loss of sulfate during evaporation. The solution from smaller samples was concentrated to a volume of 50 ml or less, and the solution to larger samples was concentrated down to a volume of ~300 – 500 ml.

Between 20 – 50 ml of the concentrated acidic solution was added to a 100 ml

boiling flask along with an equal part reduction solution (410ml HCl – JT Baker 9535-33,

245 ml HI - Sigma Aldrich 248649, 121ml H_3PO_2 - Lancaster Synthesis 14752; *e.g.*,

Thode *et al.*, 1961) and heated to reduce the sulfate in solution to H_2S. A 25 ml culture

tube containing ~15 ml 0.1 M Zn acetate trapping solution ($Zn(CH_3CO_2)_2$) was connected

to the reduction assembly to collect the resulting H_2S as ZnS. Diatomic nitrogen gas was

used as a carrier for the H_2S. Once all reduction manifolds were assembled, connections

secured and the assembly checked for leaks, the flow rate of N_2 gas was adjusted until

~1-2 bubbles per second pass through the water trap (Figure 7). The heating mantles

below the boiling flasks were then turned on to deliver enough heat to the solution to

bring it to the boiling point. The solution was heated for at least 3 hours. After the run

was complete, ~2-3 ml of 5% (w/v) silver nitrate ($AgNO_3$) solution was added to the

culture tubes that contained the Zn Acetate trapping solution. Nitrogen gas was

continuously bubbled through the trap during this procedure to ensure complete mixing

of the ZnS precipitate and the silver nitrate solution and, accordingly, quantitative

conversion of the ZnS to Ag_2S (silver sulfide).   The trap was removed from the assembly

and set aside in a darkened area for at least 24 hours. The trapping solution was vacuum

filtered, and the silver sulfide precipitate was collected on a 0.22 μm cellulose membrane

filter (Millipore e02wp02500). Samples from the lower Duitschland Formation and

Malmani required multiple extractions that were recombined in the filtering process; The

silver sulfide from each of trapping solution from the multiple flasks was filtered onto at

single filter. The silver sulfide was washed with ~150 ml Millipore water, then with ~15

ml 1M NH_4OH,
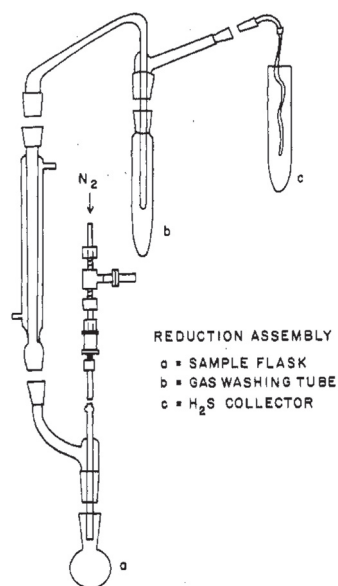
Figure 7 Apparatus setup for the carbonate-associated sulfate extraction method for trace sulfate samples (after Forrest and Newmann, 1977). Concentrated acidified sample is placed in the boiling flask (a) and heated. The H_2S gas released upon heating moves up through the condenser, is then bubbled through the gas washing tube (b), and is collected in a Zn-acetate trapping solution (c). From Forrest and Newmann, 1977.

followed by an additional wash of ~100 ml Millipore water. The silver sulfide was

removed from the filter and oven dried.

3.1.2 Chromium(II)-Reducible Sulfur Extraction

Samples with disseminated sulfide grains were processed using a method based

on techniques in Hsieh and Shieh (1997). The method uses a chromium(II) reagent

($CrCl_2 \cdot 6 H_2O$) in order to reduce sulfur in sulfide minerals to H_2S and an alkaline zinc

trapping solution ($Zn(CH_3CO_2)_2$) to sequester the sulfur in the evolved H_2S as ZnS.

Each of the diffusion containers contained two 50 ml beakers that are placed under

stopcocks in the container lids (Figure 8). One beaker contained $1 - 5$ g of the powdered

sample, and the other beaker contained ~20 ml of the alkaline zinc trapping solution. The

diffusion container was flushed with N_2, then one stopcock was closed and the container

pressurized before the second stopcock was closed. A leak test was done by waiting ~30

seconds before opening one of the stopcocks. If no leaks were found, the diffusion

container was repressurized. A luer-lock syringe was used to introduce ~15 ml of the

Cr(II) solution through the stopcock into the beaker containing the powdered sample.

The stopcock above the sample was opened, the Cr(II) solution was slowly injected, and

the stopcock closed prior to removing the syringe from the stopcock. A second luer-lock

syringe was used to inject ~15 ml of 5.0N hydrochloric acid into the sample beaker using

the same method as the injection of the Cr(II) solution. After ~48 hours, the beakers

containing the ZnS precipitate and the residual alkaline zinc trapping solution were

removed from the diffusion container and filtered through a 0.22 μm cellulose membrane

filter (Millipore e02wp02500) under a vacuum. Solids remaining on the filter were
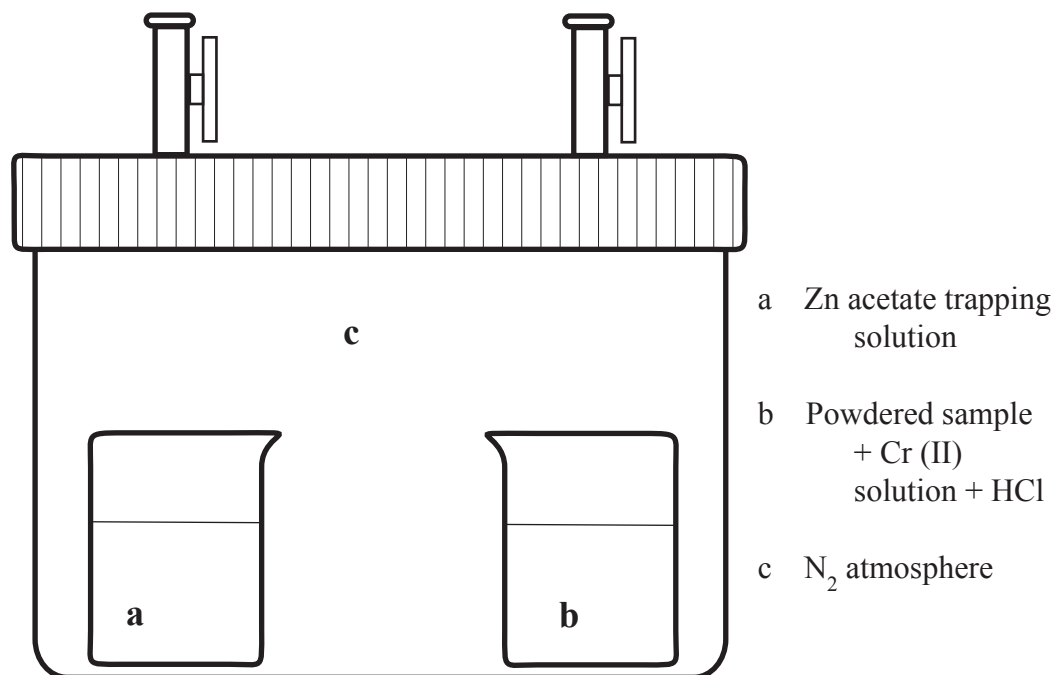
Figure 8 Apparatus for the extraction of reduced sulfur using the Cr(II) solution diffusion method after Hsieh & Shieh, 1997. Zn-acetate trapping solution is placed into one of the small beakers (a). In the other beaker is ~1 gram of powdered sample that has ~25 mL of the Cr(II) solution and ~15mL of HCl added by the luer-syringes through the stopcock above the beaker.

washed with ~150 ml Millipore water, then they were reacted with several drops of 5 % (w/v) $AgNO_3$ solution added to the filter before the vacuum was turned off. Once the vacuum was off, additional 5 % (w/v) $AgNO_3$ solution was added to the filter and left to react for ~3 minutes. The vacuum was then turned back on and the precipitate washed with ~15 ml of 1M NH_4OH followed by ~100 ml of Millipore water. The silver sulfide was removed from the filter and oven dried.

3.1.3 Mass Spectrometric Analysis for Sulfur Isotopes

Dried silver sulfide powders were weighed out into aluminum-foil boats and placed into individual nickel reaction vessels. The Ni reaction vessels (~100 ml) were evacuated, and then cooled with liquid nitrogen and then filled with purified elemental fluorine to a pressure of ~2 inches Hg (50 Torr). The reaction vessels were then heated to ~ 240 °C, and the silver sulfide powders were allowed to react with F_2 gas for ~ 8 hours to quantitatively transfer the sulfur in the sample into SF_6 gas. Residual F_2 in the reaction vessels was removed through reaction with KBr at ~100 °C. During this procedure, the SF_6 sample and any condensable impurities were transferred from the reaction vessel to a "U" trap held at the boiling point of liquid nitrogen (-196 °C). After passivation of the residual F_2, any non-condensable gases were pumped off. The "U" trap containing the SF_6 and other condensable gases was warmed up to ~115° C using ethanol cooled liquid nitrogen. This temperature allowed SF_6 to sublimate and to be separated from other condensable gases with higher boiling points. The SF_6 was then passed through a gas chromatograph, which uses a Helium carrier gas through a 1/8 inch GC column consisting of a 12' column packed with HaysepQ followed by 6' column

packed with Mol Sieve 5Å at a flow rate of ~10 ml/min, to for further purification before being introduced into the ThermoFinnigan MAT 253 dual-inlet gas source mass spectrometer for isotopic analysis. Analytical results have been normalized to the isotopic composition of Vienna-Cañon Diablo Troilite (V-CDT).

3.1.4.0 Measurement Uncertainties for Sulfur Isotopic Analysis

Measurement uncertainties were assessed in two stages. First, the errors associated with the combined fluorination and mass spectrometry procedures were quantified using a long-term database of analyses of international standards in the University of Maryland stable isotope laboratory. Operator consistency with these errors was checked by repeated analysis of an in-house Ag_2S powder. Second, processing splits of the same material allowed the errors associated with the different extraction procedures to be assessed. The overall uncertainty related to the total analytical procedure for CAS samples is estimated to be 0.266‰ for $\delta^{34}S$, 0.007‰ for $\Delta^{33}S$, and 0.15‰ for $\Delta^{36}S$. The uncertainty related to the Cr(II) reduction procedure is estimated to be 0.145‰ for $\delta^{34}S$, 0.011‰ $\Delta^{33}S$, and 0.08‰ for $\Delta^{36}S$. The reproducibility in the fluorination and mass spectrometry procedures is 0.12‰ for $\delta^{34}S$, 0.008‰ for $\Delta^{33}S$, and 0.2‰ for $\Delta^{36}S$. As the uncertainty estimated for the extraction procedures encompasses that from the fluorination and mass spectrometry, the extraction uncertainties are used in all plots and discussion. All sulfur analysis were standardized to V-CDT assuming a composition of IAEA S-1 of -0.05 $\delta^{33}S$, -0.30 $\delta^{34}S$, and -0.57 $\delta^{36}S$.

3.1.4.1 Reproducibility of fluorination and mass spectrometric procedures

Shown in Table 1 are the results of analysis of an in-house Ag_2S powder, SS-1. The variability related to fluorination is +0.147‰ for $\delta^{34}S$, +0.002‰ $\Delta^{33}S$, and +0.09‰ for $\Delta^{36}S$.

Table 1 Sample Repeats to Establish Experimental Reproducibility for Fluorination

	$\delta^{34}S_{V\text{-}CDT}$	$\delta^{33}S_{V\text{-}CDT}$	$\delta^{36}S_{V\text{-}CDT}$	$\Delta^{33}S_{V\text{-}CDT}$	$\Delta^{36}S_{V\text{-}CDT}$
SS1-A	2.817	5.431	10.88	0.024	0.48
SS1-B	2.763	5.319	10.53	0.027	0.34
SS1-C	2.912	5.611	11.24	0.027	0.50
Average	2.831	5.454	10.88	0.026	0.44
Mean SDV (1σ)	0.076	0.147	0.36	0.002	0.09

3.1.4.2 Reproducibility of sulfate reduction extraction procedure

Reproducibility was analyzed for sulfate reductions by processing two samples of NB127, an isotopic standard consisting of purified $BaSO4$. Two samples of NBS127 were taken through the CAS extraction procedure at amount representative of the sulfur content in the field samples. A third sample, with mass 0.285 milligrams, was processes in order to determine the isotopic consequences of extracting sulfur from small samples. As Table 2 shows, this sample is likely to have been fractionated in the reduction procedure relative to the accepted isotopic composition of NBS127.

Table 2 Sample Repeats to Establish Experimental Reproducibility for CAS Extraction

	mass (mg)	$\delta^{34}S_{V\text{-}CDT}$	$\delta^{33}S_{V\text{-}CDT}$	$\delta^{36}S_{V\text{-}CDT}$	$\Delta^{33}S_{V\text{-}CDT}$	$\Delta^{36}S_{V\text{-}CDT}$
NBS127A	1.792	21.794	11.205	41.60	0.040	-0.44
NBS127B	*0.285*	*17.780*	*9.123*	*34.477*	*0.006*	*0.24*
NBS127C	21.903	21.433	11.012	40.73	0.030	-0.61
Average		21.614	11.109	41.17	0.035	-0.52

3.1.4.3 Reproducibility of the Cr(II)-reducible sulfide extraction procedure

Reproducibility was analyzed for the Cr(II)-reducible sulfide extraction procedure by processing five ~1 gram samples of DF03-P.   This procedure resulted in a reproducibility of +0.123‰ for δ^{34}S, +0.011‰ for Δ^{33}S, and +0.075‰ for Δ^{36}S (Table 3). These values are taken as the uncertainty of a single analysis that is taken through the Cr(II)-reducible sulfide extraction procedure.

Table 3 Sample Repeats to Establish Experimental Reproducibility for Cr(II) Extraction

	δ^{34}S$_{V\text{-}CDT}$	δ^{33}S$_{V\text{-}CDT}$	δ^{36}S$_{V\text{-}CDT}$	Δ^{33}S$_{V\text{-}CDT}$	Δ^{36}S$_{V\text{-}CDT}$
DF03-P	**4.622**	**3.654**	**7.12**	**1.276**	**-1.73**
DF03-PA	4.549	3.637	7.02	1.297	-1.69
DF03-PB	4.599	3.669	7.10	1.303	-1.70
DF03-PC	4.335	3.519	6.56	1.289	-1.73
DF03-PD	4.390	3.540	6.53	1.282	-1.87
DF03-PE	4.596	3.640	6.99	1.276	-1.80
Average	4.440	3.567	6.70	1.283	-1.80
Mean SDV (1σ)	0.123	0.067	0.27	0.011	0.08

3.2.0 Carbon and Oxygen Isotopic Analysis

Billets of carbonate samples were cut and polished for the carbonates samples collected for this study. The billets were evaluated for secondary recrystallization using a Luminoscope cathodoluminescence chamber. Recrystallized carbonates with higher manganese will show a brighter luminosity than carbonate with lower manganese (Machel & Burton, 1991; Machel *et al.*, 1991). Photographs were taken of samples showing luminescence to locate micro-drilling sites within each sample (Fig. 9).
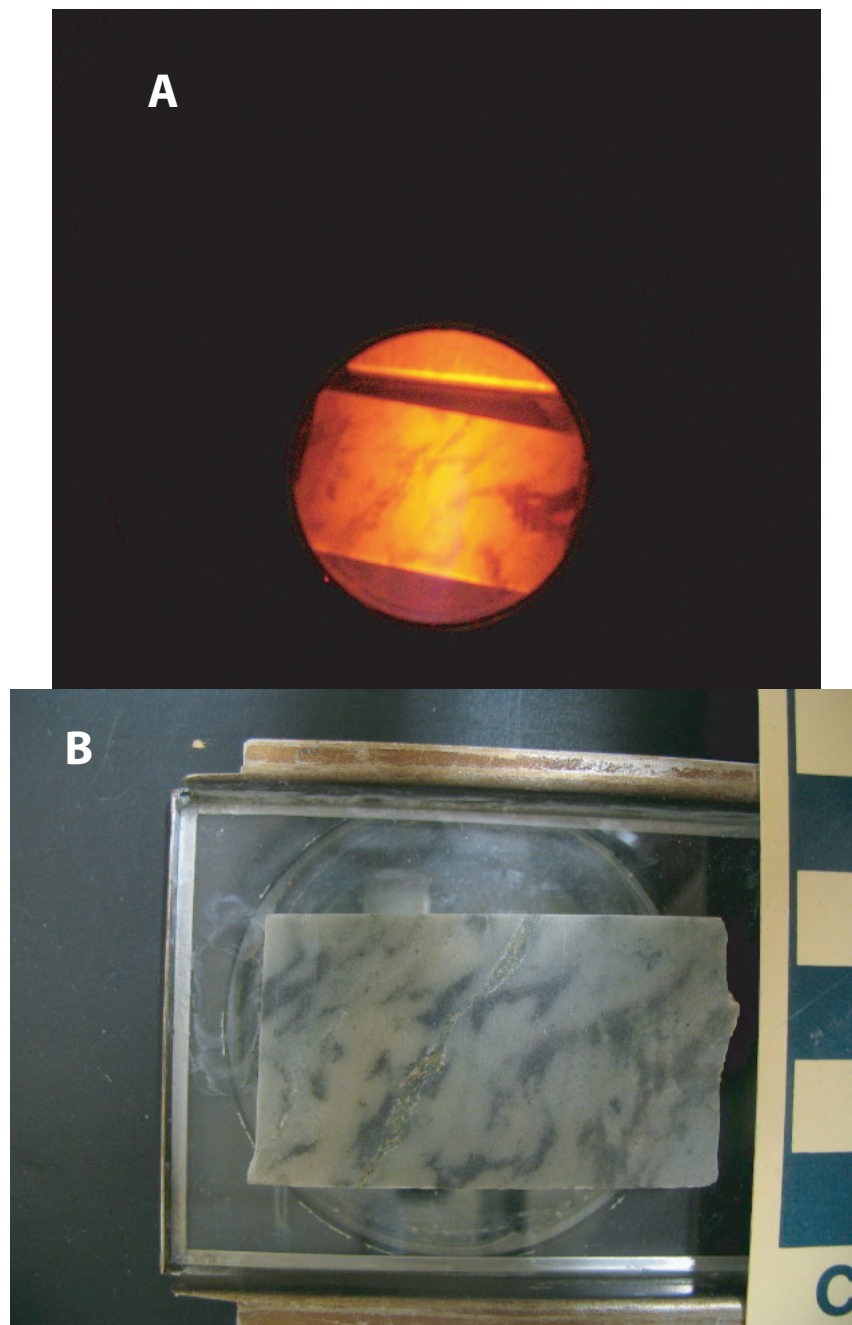
Figure 9 Representative photographs of the carbonate billets examined using a Luminoscope cathodoluminescence chamber for post diagenetic recrystallization. Photograph A shows samples DF08-C in the Luminoscope cathodoluminescence chamber. Photograph B shows the same sample with a cm scale on the right side that is on top of the chamber window. Note that there is almost no noticeable variation in the sample that would be not expected when examining the handle samples.

Locations with low luminescence and no visible veins were selected for micro-drilling to produce rock powder for carbon and oxygen isotopic analysis. One hundred (±20) µg of the micro-drilled powders were weighed out for each sample and placed into a WheatonV-vial that was topped with a Kel-F disc and a rubber septum underneath the vial cap.

3.2.1.0 Mass Spectrometric Analysis of Carbon and Oxygen Isotopes

Samples from this study were run along with several repeats of NBS19, a powdered calcite that is an international standard for carbon and oxygen isotopes. The vials were placed into a temperature-controlled autosampling rack and heated to ~90 °C. The septum on top of each vial was punctured by a double needle. The vial was evacuated through the outer needle and then 102% phosphoric acid (H_3PO_4) was added through the inner needle. The H_3PO_4 was allowed to react with the sample for ~10 minutes while evolved CO_2 was transferred to a trap cooled by liquid nitrogen. Depending on amount of CO_2 produced, the gas was transferred either to the sample bellows or a cold finger before introduction to the Micromass IsoPrime dual-inlet gas source mass spectrometer for isotope analysis. Isotopic compositions were normalized to the Vienna PeeDee Belemnite scale (V-PDB) using analyses of NBS-19.

3.2.1.1 Analytical Uncertainties for Carbon and Oxygen Isotopic Analysis

External reproducibility of analysis on the Micromass IsoPrime dual-inlet gas source mass spectrometer was calculated using the 7 analyses of NBS19 that were used for standardization of the run. Shown in Table 4 are the results of analyses and the

National Institute of Standard and Technology (NIST) published $\delta^{13}C_{V\text{-}PDB}$ and $\delta^{18}O_{V\text{-}PDB}$ values.

Table 4 External Reproducibility of International Standards

		$\delta^{13}C_{V\text{-}PDB}$	$\delta^{18}O_{V\text{-}PDB}$	$\delta^{13}C_{V\text{-}PDB}$	$\delta^{18}O_{V\text{-}PDB}$
		NIST	NIST		
NBS19-A				1.894	-2.174
NBS19-B				1.990	-2.143
NBS19-C				1.995	-2.108
NBS19-D				1.990	-2.221
NBS19-E				1.861	-2.351
NBS19-F				1.969	-2.187
NBS19-G				1.952	-2.215
Accepted Value		1.950	-2.200		
Mean SDV (1σ)				0.053	0.077

3.3 Stratigraphic Column Assignment

Global Positioning System (GPS) coordinates for each sample were recorded; however, two different GPS handheld receivers were used at different times, with one recording positions in latitude and longitude and the other using Northing and Easting. All positions were translated into Northing and Easting using software developed by Steve Dutchs at the University of Wisconsin-Green Bay (http://www.uwgb.edu/dutchs/UsefulData/UTMFormulas.HTM). This conversion is in part because the software accuracy is better at converting from latitude and longitude to Northing and Easting, removing the need for an additional conversion from latitude and

longitude to meter. Shown in Table 5 are the positions of the samples in both coordinate

systems as well as any strike and dip readings taken in the field.

Once the sample position was converted to meters, the distance from the sample

position was calculated based on its place relative to DF28-P from the Penge Banded

Ironstone Formation (BIF). This sample was used as the reference datum point because

the coordinates of a true stratigraphic contact were not measured in the field. The Penge

BIF is thin relative to the surrounding Duitschland Formation and Malmani Subgroup at

Duitschland Farm; therefore, referencing the column to DF28-P introduces the least

amount of absolute uncertainty in the stratigraphic position of the different samples. The

difference between the sample position and DF28-P was used to project the sample

position on a horizontal line perpendicular to the average strike of 170°. This depth is

then corrected for an average dip of 32°S using the equation, $Y = X \cos 32°$ to assign a

final stratigraphic height to the sample. The error from the strike and dip measurements

was propagated from each step to provide an overall error of the stratigraphic depth and

the minimum value shown in Table 6.

In addition to samples from the Duitschland Formation and Penge BIF, samples

were also collected from the Malmani Subgroup. The positions of these samples were

also calculated as mentioned above. These samples have a negative depth in relationship

to the Penge BIF, because the Penge BIF overlies the Malmani Subgroup. The calculated

stratigraphic positions of the Duitschland Formation samples were correlated to the

Bekker *et al.* (2001) stratigraphic column. However, the decision to reference the

samples for this study to DF28-P introduces a fixed uncertainty in the position of the

entire stratigraphic column because the position of DF28-P within the Penge BIF is not

known. This uncertainty of position within the Penge BIF means that the assigned

stratigraphic heights for this study could be off as much as the thickness of the Penge BIF

in the study area.

Table 5 Field Data for Duitschland Farm Samples

sample	strike	dip	longitude	latitude	easting	northing
DF01-P	175°	34°	E29° 8' 12"	S24° 17' 51"	716854 E	7311172 N
DF02-P			E29° 8' 11"	S24° 17' 56"	716823 E	7311018 N
DF03-P			E29° 8' 11"	S24° 17' 55"	716823 E	7311049 N
DF04-P	169°	30°	E29° 8' 10"	S24° 17' 52"	716797 E	7311142 N
DF05-P	165°	29°	E29° 8' 6"	S24° 17' 46"	716687 E	7311328 N
DF06-P			E29° 8' 1"	S24° 17' 44"	716547 E	7311392 N
DF07-P			E29° 7' 48"	S24° 17' 29"	716187 E	7311859 N
DF08-C			E29° 7' 49"	S24° 17' 30"	716215 E	7311828 N
DF09-C			E29° 7' 50"	S24° 17' 31"	716243 E	7311797 N
DF10-C			E29° 7' 44"	S24° 17' 28"	716075 E	7311892 N
DF11-P			E29° 7' 40"	S24° 17' 28"	715962 E	7311893 N
DF12-P	181°	36°	E29° 7' 38"	S24° 17' 28"	715905 E	7311863 N
DF13-C	157°	31°	E29° 7' 38"	S24° 17' 30"	715905 E	7311833 N
DF14-C			E29° 7' 37"	S24° 17' 28"	715877 E	7311895 N
DF15-C			E29° 7' 30"	S24° 17' 32"	715678 E	7311775 N
DF16-C			E29° 7' 33"	S24° 17' 33"	715762 E	7311742 N
DF17-C					716855 E	7310189 N
DF18-C					716775 E	7310324 N
DF19-C					716202 E	7310822 N
DF20-C					716182 E	7310820 N
DF21-C					715637 E	7311929 N
DF22-C					715644 E	7311915 N
DF23-C					717760 E	7310556 N
DF24-C					718869 E	7310847 N
DF25-C					718583 E	7310833 N
DF26-C					718327 E	7310697 N
DF27-C					718112 E	7310715 N
DF28-P					717528 E	7310664 N
TR101-C			E29° 54' 42"	S24° 10' 52"	795818 E	7322642 N
TR102-C			E29° 54" 41"	S24° 10' 54"	795788 E	7322581 N
average	170.2°	32°				
SDV	±8.9	±2.9				

Table 6 Stratigraphic Position and Error for Duitschland Farm Samples

sample	Depth (m)	error (m)
DF01-P	398	±64
DF02-P	400	±67
DF03-P	403	±67
DF04-P	425	±69
DF05-P	499	±80
DF06-P	578	±93
DF07-P	808	±128
DF08-C	791	±126
DF09-C	773	±123
DF10-C	870	±139
DF11-P	929	±149
DF12-P	956	±155
DF13-C	953	±155
DF14-C	973	±157
DF15-C	1066	±175
DF16-C	1019	±167
DF17-C	309	±61
DF18-C	363	±69
DF19-C	707	±123
DF20-C	717	±125
DF21-C	1102	±180
DF22-C	1097	±179
DF23-C	-131	±22
DF24-C	-684	±124
DF25-C	-536	±97
DF26-C	-414	±74
DF27-C	-300	±54
DF28-P	0	0

4.0 Results

Samples from this study were collected from Duitschland Farm 95KS, located southwest of Mokopane (formally Potgietersrus), South Africa, and include field samples from the Malmani Subgroup, the Penge Banded Ironstone Formation (BIF), and the Duitschland Formation. Additional samples from the Tongwane Formation, which is not well preserved in the Duitschland Farm area, were collected at the Tongwane River valley to the northeast of the farm. Table 7 includes the sample number, calculated stratigraphic positions, and analytical results of samples from this study. The lithology of the sample is indicated by the letter after the sample number. Carbonate samples are designated with the letter "C" indicating carbonate samples and pelitic (shale) samples are designated by the letter "P".   A total of 30 samples were collected for analysis: 20 carbonates and 10 shales.

The Malmani Subgroup samples (n=5) are cherty carbonates that are primarily laminated dolomites interbedded with cherty layers ranging from 25-50 cm. The sample from the Penge BIF is a layered phyllite containing siderite ($FeCO_3$) and hematite (Fe_2O_3). The Duitschland Formation samples (n=22) are primarily pelitic in the lower section and primarily carbonates in the upper section. The middle section of the Duitschland Formation is poorly exposed in a valley between hills of the well exposed lower and upper sections. No stratigraphic position was calculated for the Tongwane Formation samples (n=2) due to the limited preservation of the formation in the Transvaal Supergroup besides assigning its position in the regional stratigraphy between

Sample	Depth (m)		$\delta^{33}S_{V\text{-}CDT}$ (‰)	$\delta^{34}S_{V\text{-}CDT}$ (‰)	$\delta^{36}S_{V\text{-}CDT}$ (‰)	$\Delta^{33}S_{V\text{-}CDT}$ (‰)	$\Delta^{36}S_{V\text{-}CDT}$ (‰)	$\delta^{13}C_{carb}$ (‰, V-PDB)	$\delta^{18}O_{carb}$ (‰, V-PDB)
DUITSCHLAND FORMATION									
DF21-C	1102	1	12.870	25.049	49.30	0.047	0.91	**6.54**	**-19.64**
		2	12.854	25.045	49.15	0.033	0.77		
		3	12.858	25.035	49.25	0.042	0.89		
		average	**12.861**	**25.0434**	**49.23**	**0.041**	**0.86**		
		SDV (1σ)	0.008	0.007	0.08	0.007	0.08		
DF22-C	1097	1	8.493	16.460	32.15	0.050	0.48	**6.05**	**-15.98**
		2	8.472	16.434	32.19	0.042	0.57		
		3	8.459	16.427	32.17	0.033	0.56		
		average	**8.475**	**16.441**	**32.17**	**0.041**	**0.53**		
		SDV (1σ)	0.017	0.017	0.02	0.009	0.05		
DF15-C	1066	1	10.535	20.440	40.05	0.060	0.65	**7.81**	**-13.42**
		2	10.520	20.431	39.95	0.050	0.57		
		3	10.516	20.438	39.95	0.042	0.55		
		average	**10.524**	**20.437**	**39.99**	**0.051**	**0.59**		
		SDV (1σ)	0.010	0.005	0.06	0.009	0.05		
DF16-C	1019	1	8.317	16.137	31.56	0.039	0.51	**6.50**	**-13.36**
		2	8.322	16.145	31.71	0.040	0.65		
		3	8.315	16.144	31.49	0.033	0.43		
		average	**8.318**	**16.142**	**31.58**	**0.037**	**0.53**		
		SDV (1σ)	0.004	0.004	0.11	0.004	0.11		
DF14-C	973	1	11.966	23.287	45.72	0.040	0.77	**1.62**	**-14.02**
		2	11.961	23.286	45.54	0.036	0.59		
		3	11.972	23.286	45.63	0.046	0.68		
		average	**11.967**	**23.286**	**45.63**	**0.041**	**0.68**		
		SDV (1σ)	0.006	0.001	0.09	0.0056	0.09		

Sample	Depth (m)		$\delta^{33}S_{V-CDT}$ (‰)	$\delta^{34}S_{V-CDT}$ (‰)	$\delta^{36}S_{V-CDT}$ (‰)	$\Delta^{33}S_{V-CDT}$ (‰)	$\Delta^{36}S_{V-CDT}$ (‰)	$\delta^{13}C_{carb}$ (‰, V-PDB)	$\delta^{18}O_{carb}$ (‰, V-PDB)
DF13-C	953	1	12.443	24.116	47.15	0.095	0.59	**2.45**	**-10.39**
		2	12.427	24.100	47.05	0.087	0.51		
		3	12.429	24.104	47.04	0.087	0.50		
		average	**12.433**	**24.107**	**47.08**	**0.090**	**0.53**		
		SDV (1σ)	0.009	0.008	0.06	0.005	0.05		
DF10-C	870	1	14.235	27.726	54.44	0.051	0.82	**3.75**	**-18.39**
		2	14.209	27.699	54.25	0.039	0.68		
		3	14.216	27.689	54.29	0.051	0.74		
		average	**14.220**	**27.705**	**54.33**	**0.047**	**0.75**		
		SDV (1σ)	0.013	0.019	0.10	0.007	0.07		
DF08-C	791	1	14.269	27.581	54.04	0.158	0.71	**6.14**	**-16.67**
		2	14.254	27.574	54.02	0.146	0.69		
		3	14.250	27.577	54.03	0.141	0.69		
		average	**14.257**	**27.577**	**54.028**	**0.149**	**0.696**		
		SDV (1σ)	0.010	0.003	0.015	0.009	0.009		
DF09-C	773	1	14.113	27.190	53.196	0.202	0.622	**5.31**	**-17.00**
		2	14.109	27.204	53.365	0.190	0.763		
		3	14.102	27.201	53.430	0.185	0.835		
		average	**14.108**	**27.198**	**53.330**	**0.192**	**0.740**		
		SDV (1σ)	0.006	0.007	0.121	0.008	0.108		
DF20-C	717	1	21.691	42.303	83.255	0.123	0.903		
		2	21.695	42.303	83.281	0.128	0.929		
		3	21.683	42.292	83.194	0.121	0.864		
		average	**21.690**	**42.299**	**83.243**	**0.124**	**0.899**		
		SDV (1σ)	0.006	0.006	0.045	0.003	0.033		

Sample	Depth (m)		$\delta^{33}S_{V\text{-}CDT}$ (‰)	$\delta^{34}S_{V\text{-}CDT}$ (‰)	$\delta^{36}S_{V\text{-}CDT}$ (‰)	$\Delta^{33}S_{V\text{-}CDT}$ (‰)	$\Delta^{36}S_{V\text{-}CDT}$ (‰)	$\delta^{13}C_{carb}$ (‰, V-PDB)	$\delta^{18}O_{carb}$ (‰, V-PDB)
DF19-C	707	1	14.556	28.268	55.52	0.097	0.83	**6.00**	**-16.16**
		2	14.559	28.271	55.44	0.098	0.75		
		3	14.564	28.277	55.33	0.100	0.62		
		average	**14.560**	**28.272**	**55.43**	**0.098**	**0.73**		
		SDV (1σ)	0.004	0.005	0.10	0.002	0.11		
DF05-P	499	1	1.762	2.350	4.63	0.552	0.14		
		2	1.756	2.347	4.64	0.549	0.15		
		3	1.750	2.353	4.77	0.539	0.27		
		average	**1.756**	**2.350**	**4.68**	**0.547**	**0.19**		
		SDV (1σ)	0.006	0.003	0.08	0.006	0.07		
DF04-P	425	1	3.266	4.009	6.67	1.204	-1.00		
		2	3.246	3.974	6.85	1.202	-0.75		
		3	3.220	3.980	6.82	1.173	-0.79		
		4	3.239	3.992	7.04	1.185	-0.60		
		5	3.234	3.973	6.88	1.190	-0.72		
		6	3.252	3.987	6.78	1.201	-0.85		
		average	**3.243**	**3.985**	**6.84**	**1.193**	**-0.79**		
		SDV (1σ)	0.016	0.014	0.12	0.012	0.13		
DF03-P	403	1	3.647	4.579	7.92	1.292	-0.85		
		2	3.623	4.555	7.76	1.280	-0.96		
		3	3.627	4.55	7.81	1.286	-0.90		
		average	**3.632**	**4.561**	**7.83**	**1.286**	**-0.90**		
		SDV (1σ)	0.013	0.015	0.08	0.006	0.06		
DF02-P	400	1	0.661	-1.462	-3.94	1.414	-1.15		
		2	0.668	-1.459	-3.91	1.420	-1.12		
		3	0.673	-1.446	-3.79	1.418	-1.03		
		average	**0.667**	**-1.456**	**-3.88**	**1.417**	**-1.10**		
		SDV (1σ)	0.006	0.009	0.08	0.003	0.06		

Sample	Depth (m)		$\delta^{33}S_{V\text{-}CDT}$ (‰)	$\delta^{34}S_{V\text{-}CDT}$ (‰)	$\delta^{36}S_{V\text{-}CDT}$ (‰)	$\Delta^{33}S_{V\text{-}CDT}$ (‰)	$\Delta^{36}S_{V\text{-}CDT}$ (‰)	$\delta^{13}C_{carb}$ (‰, V-PDB)	$\delta^{18}O_{carb}$ (‰, V-PDB)
DF01-P	398	1	3.348	5.322	12.35	0.611	2.16		
		2	3.332	5.420	10.06	0.544	-0.32		
		3	3.381	5.340	9.96	0.635	-0.26		
		average	**3.354**	**5.360**	**10.79**	**0.597**	**0.53**		
		SDV (1σ)	0.025	0.052	1.35	0.047	1.42		
DF18-C	363	1	3.397	6.171	12.50	0.223	0.68	**0.01**	**-10.03**
		2	3.393	6.163	12.39	0.224	0.58		
		3	3.362	6.168	12.45	0.191	0.64		
		average	**3.384**	**6.167**	**12.44**	**0.213**	**0.63**		
		SDV (1σ)	0.019	0.004	0.05	0.019	0.05		
DF17-C	309	1	6.481	11.117	21.16	0.771	-0.18	**-1.71**	**-11.02**
		2	6.476	11.117	21.29	0.766	-0.05		
		3	6.477	11.125	21.46	0.763	0.10		
		average	**6.478**	**11.119**	**21.30**	**0.767**	**-0.04**		
		SDV (1σ)	0.003	0.005	0.15	0.004	0.14		

PENGE BANDED IRONSTONE FORMATION

Sample	Depth (m)		$\delta^{33}S_{V\text{-}CDT}$ (‰)	$\delta^{34}S_{V\text{-}CDT}$ (‰)	$\delta^{36}S_{V\text{-}CDT}$ (‰)	$\Delta^{33}S_{V\text{-}CDT}$ (‰)	$\Delta^{36}S_{V\text{-}CDT}$ (‰)	$\delta^{13}C_{carb}$ (‰, V-PDB)	$\delta^{18}O_{carb}$ (‰, V-PDB)
DF28-P	0	1	2.973	5.416	10.75	0.187	0.38		
		2	3.005	5.430	10.61	0.212	0.21		
		3	2.984	5.445	10.74	0.184	0.32		
		average	**2.987**	**5.430**	**10.70**	**0.194**	**0.30**		
		SDV (1σ)	0.016	0.014	0.08	0.015	0.08		

Sample	Depth (m)		$\delta^{33}S_{V\text{-}CDT}$ (‰)	$\delta^{34}S_{V\text{-}CDT}$ (‰)	$\delta^{36}S_{V\text{-}CDT}$ (‰)	$\Delta^{33}S_{V\text{-}CDT}$ (‰)	$\Delta^{36}S_{V\text{-}CDT}$ (‰)	$\delta^{13}C_{carb}$ (‰, V-PDB)	$\delta^{18}O_{carb}$ (‰, V-PDB)
MALMANI SUBGROUP									
DF23-C	-131	1	6.408	10.453	20.43	1.039	0.37	**-1.03**	**-10.19**
		2	6.419	10.455	20.28	1.049	0.22		
		3	6.440	10.455	20.25	1.070	0.18		
		average	**6.422**	**10.454**	**20.32**	**1.052**	**0.26**		
		SDV (1σ)	0.016	0.001	0.10	0.016	0.10		
DF27-C	-300	1	9.076	14.437	27.08	1.667	-0.67	**-0.53**	**-10.18**
		2	9.062	14.412	27.07	1.665	-0.63		
		3	9.049	14.392	26.89	1.662	-0.78		
		4	9.087	14.474	27.06	1.659	-0.76		
		average	**9.068**	**14.429**	**27.03**	**1.663**	**-0.71**		
		SDV (1σ)	0.0166	0.0352	0.09	0.004	0.07		
DF26-C	-414	1	8.443	10.913	19.39	2.838	-1.56	**-0.30**	**-9.79**
		2	8.471	10.914	19.47	2.865	-1.48		
		3	8.454	10.920	19.67	2.845	-1.29		
		average	**8.456**	**10.915**	**19.51**	**2.849**	**-1.44**		
		SDV (1σ)	0.014	0.004	0.15	0.014	0.14		
TONGWANE FORMATION									
TR01-C		1	9.619	18.516	36.41	0.126	0.75	**-0.56**	**-8.73**
		2	9.630	18.526	36.49	0.132	0.81		
		3	9.632	18.516	36.50	0.139	0.83		
		average	**9.627**	**18.520**	**36.47**	**0.132**	**0.80**		
		SDV (1σ)	0.007	0.006	0.05	0.007	0.04		

the Penge BIF and the Duitschland Formation. Post diagenetic alteration was qualified by cathodoluminscence.

Not all field samples collected were analyzed for sulfur, carbon, and oxygen isotopic data. As discussed in the previous section on Analytical Methods, sulfur was extracted from carbonate rich samples by using the carbonate associated sulfate procedure, referred to as "sulfate" samples, and sulfur was extracted from pelitic samples by using a Chromium (II) reduction procedure, referred to as "sulfide" samples. Sulfur extraction on several of the pelite samples (n=4) were attempted without success with different amounts of starting rock powder. Samples DF06-P and DF07-P are from the upper portion lower section of the Duitschland Formation, and samples DF11-P and DF12-P are the only pelites in the upper section of the Duitschland Formation. Initial attempts to extract sulfur from DF24-C and DF25-C from the Malmani Formation and sample TR02-C from the Tongwane Formation with the standard 25g of rock powder were not success and additional attempts were not completed. Figure 10 shows the sulfur and carbon isotopic values for study samples compared to their stratigraphic position.
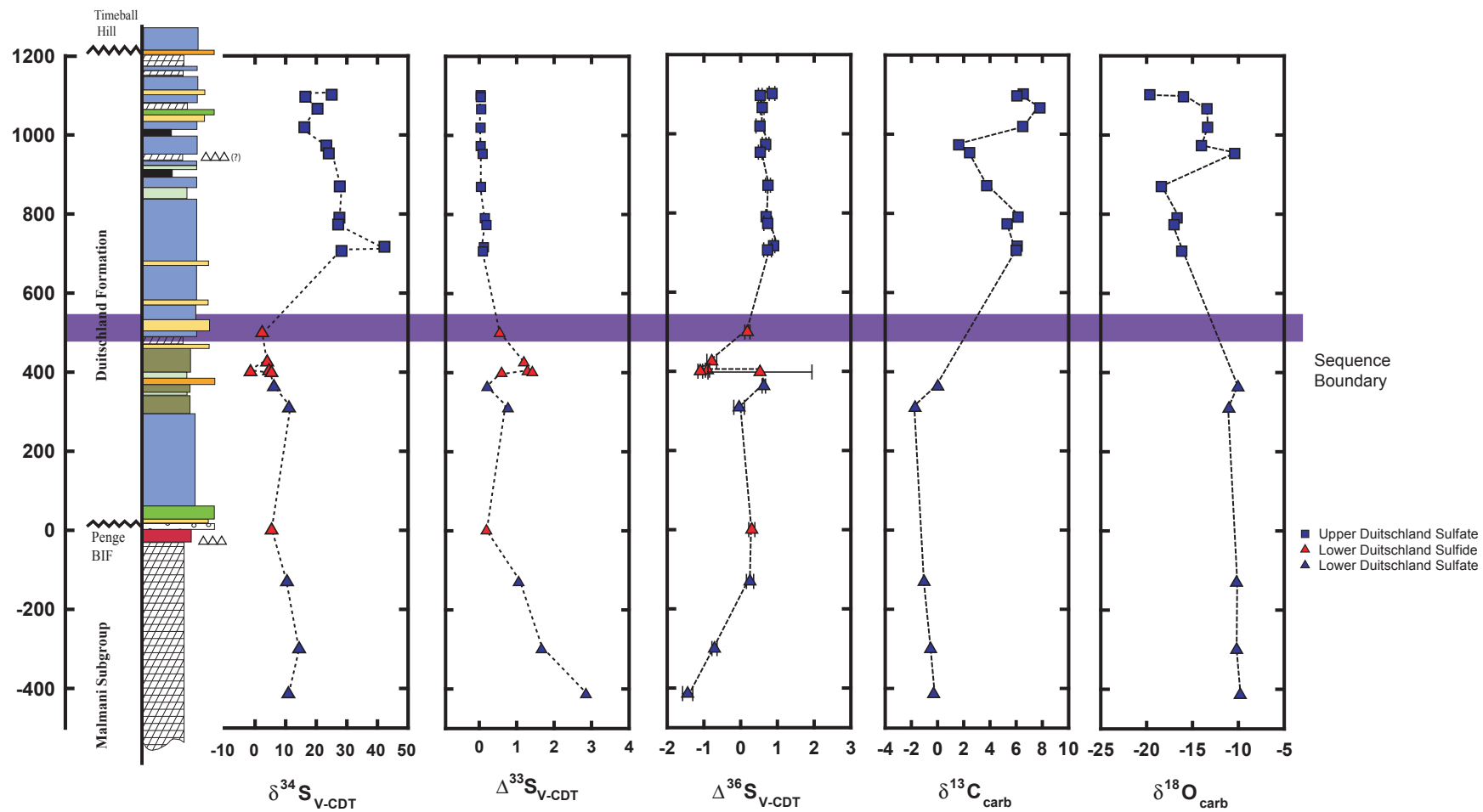
4.1.0 Sulfur Isotopic Data

4.1.1 δ^{34}S Isotopic Data

The δ^{34}S isotopic values (‰) of both sulfate and sulfide samples overall systematically increase from the base of the Malmani Subgroup through the Penge Banded Ironstone Formation and into the upper portion of the Duitschland Formation (Fig. 10). Within sections of each of the formations, there are oscillations that are likely

in response to paleoenvironmental changes. Samples from the Malmani Subgroup (n=3) have $\delta^{34}S$ isotopic values that range from +10.45 to +14.43. The Penge BIF sample (n=1) has a $\delta^{34}S$ value of +5.43. The Tongwane Formation sample (n=1) has a $\delta^{34}S$ value of +18.52. The Duitschland Formation samples (n=18) have $\delta^{34}S$ values ranging from -1.46 to +42.30. Sulfide samples from the lower Duitschland Formation range in $\delta^{34}S$ values from -1.46 to +5.36 and the two carbonate samples lower than these pelites are more positive with DF18-C having a $\delta^{34}S$ value of +6.17 and DF17-C having a $\delta^{34}S$ value of +11.12. Collectively, the samples from the Malmani Subgroup, the Penge BIF, and the lower Duitschland Formation show a similar range of $\delta^{34}S$ values and indicate small values for fractionation between coeval sulfate and sulfide samples. Carbonate samples from the upper Duitschland Formation (n=11) range in $\delta^{34}S$ values from +16.14 to +45.63.

4.1.2 $\Delta^{33}S$ Isotopic Data

The $\Delta^{33}S$ isotopic values (‰) systematically decrease from the base of the study sequence to its top, with a range of +2.85 to +0.04 (Fig. 10). Within sections of each of the formations, there are oscillations that are likely in response to paleoenvironmental changes. The Malmani Subgroup (n=3) samples have $\Delta^{33}S$ isotopic values ranging +1.05 (n=18) have $\Delta^{33}S$ values ranging from +1.42 to +0.04. Sulfide samples from the lower Duitschland Formation record the largest positive $\Delta^{33}S$ values in the formation, ranging from +1.42 to +0.55, and the two underlying carbonate samples record similarly positive values, with DF18-C having a $\Delta^{33}S$ value of +0.21 and DF17-C having a $\Delta^{33}S$ value of +0.77. The samples from the Malmani Subgroup, the Penge BIF, and the lower

Timeball
Hill

Duitschland Formation

Penge
BIF

Malmani Subgroup

$\delta^{34}S_{V\text{-}CDT}$

$\Delta^{33}S_{V\text{-}CDT}$

$\Delta^{36}S_{V\text{-}CDT}$

$\delta^{13}C_{carb}$

$\delta^{18}O_{carb}$

Sequence
Boundary

■ Upper Duitschland Sulfate
▲ Lower Duitschland Sulfide
▲ Lower Duitschland Sulfate

Duitschland Formation show Δ^{33}S values greater than +0.10. Four carbonates from the

lower portion of the upper Duitschland Formation – DF19-C, DF20-C, DF09-C and

DF08-C – also record Δ^{33}S values above +0.10, ranging in Δ^{33}S values from +0.10 to

+0.19. The remaining carbonate samples above this point have Δ^{33}S values ranging from

+0.04 to +0.09. A striking feature of the data is the presence of significant nonzero Δ^{33}S

values for samples below DF05-P that is 499m above the Penge BIF sample (DF28-P),

and absence of significant nonzero Δ^{33}S values for samples including and above DF19-C

that is 707m above the Penge BIF sample.

4.1.3 Δ^{36}S Isotopic Data

The Δ^{36}S isotopic values (‰) of both sulfate and sulfide samples overall

systematically increase from the base of the Malmani Subgroup through the Penge

Banded Ironstone Formation and into the upper portion of the Duitschland Formation

(Fig. 10). Within sections of each of the formations, there are oscillations that are likely

in response to paleoenvironmental changes. The Malmani Subgroup (n=3) samples have

Δ^{36}S isotopic values ranging -1.4 to +0.3. The Penge BIF sample (n=1) has a Δ^{36}S value

of +0.3. The Tongwane Formation sample (n=1) has a Δ^{36}S value of +0.8. The

Duitschland Formation samples (n=18) have Δ^{36}S values ranging from -1.1 to +0.9.

Sulfide samples from the Duitschland Formation record the largest negative Δ^{36}S values

Figure 10 Isotopic plot of Sulfur, Carbon, and Oxygen values for samples against their stratigraphic position. The simplified stratigraphic column is modified from Bekker *et al.* (2001). The erosional sequence boundary in the Duitschland Formation is ~400m above the basal contact with the Penge Banded Ironstone Formation.

in the formation, ranging from -1.1 to +0.5. The two underlying carbonate samples recorded +0.6 and -0.4, respectively for DF18-C and DF17-C. The remaining carbonate samples from the upper Duitschland Formation have positive $\Delta^{36}S$ values ranging from +0.5 to +0.9.

4.1.4 Correlations Between Sulfur Isotopic Data

Figure 11 shows the range of $\Delta^{33}S$ values compared to $\delta^{34}S$ values for this study and for Archean and Paleoproterozoic samples from the literature (Ono *et al.*, 2003, Mojzsis *et al.*, 2003, Bekker et al, 2004). Samples from the Malmani Subgroup, the Penge BIF, and the lower Duitschland Formation span a small range of $\delta^{34}S$ values (<15‰). Samples below DF05-P also record the highest $\Delta^{33}S$ values in the series. Fractionation between sulfate values and coeval sulfide samples ranges from close to zero to ~10‰. All sulfide samples are more negative than the sulfate samples in $\delta^{34}S$ values. Samples from the upper Duitschland Formation span a much wider range of $\delta^{34}S$ values (>15‰) and record larger ^{34}S enrichments than those reported in previous studies. However, the samples from this study with non-zero $\Delta^{33}S$ values have more positive $\delta^{34}S$ values than coeval samples from other basins.

The $\Delta^{33}S$ and $\Delta^{36}S$ values for these samples are inversely correlated, with samples that have the more positive $\Delta^{33}S$ values having the more negative $\Delta^{36}S$ values and samples from the upper Duitschland Formation that have close to zero $\Delta^{33}S$ values having $\Delta^{36}S$ values also near zero. Samples from the Malmani Subgroup have $\Delta^{33}S$ and $\Delta^{36}S$ values that range from +1.05 to +2.85 and -1.4 to +0.3, respectively. The Penge BIF sample has a $\Delta^{33}S$ value of +0.19 and a $\Delta^{36}S$ value of +0.3. The Tongwane Formation

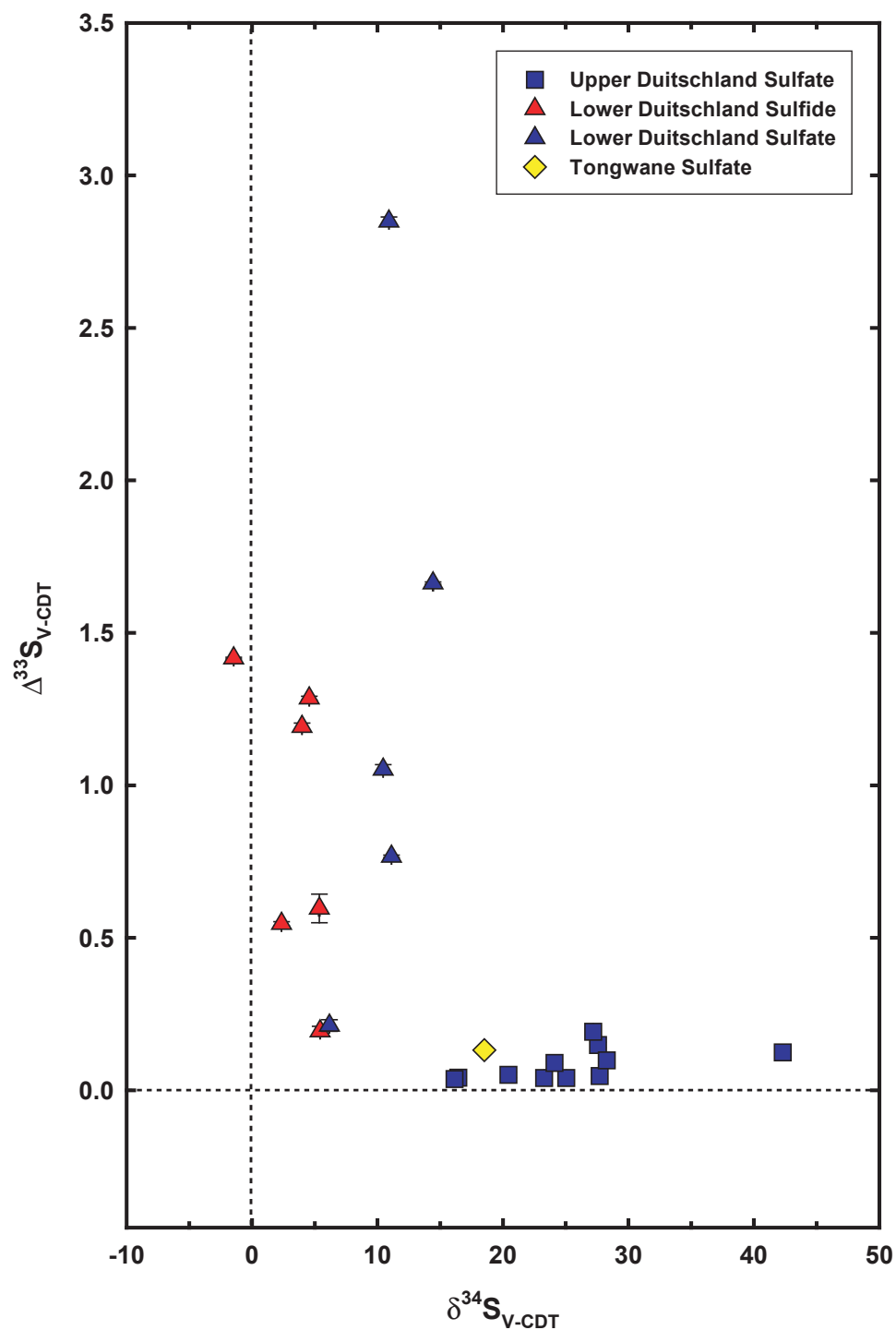**Figure 11** Isotopic plot of $\delta^{34}S$ values against $\Delta^{33}S$ values for all samples from this study. Samples from the Lower Duitschland Formation and below show a wide range of $\Delta^{33}S$ values and a limited range of $\delta^{34}S$ values. The Upper Duitschland sulfate samples show a small range of $\Delta^{33}S$ values and a wide range of $\delta^{34}S$ values. Errors are smaller than symbols for most samples.
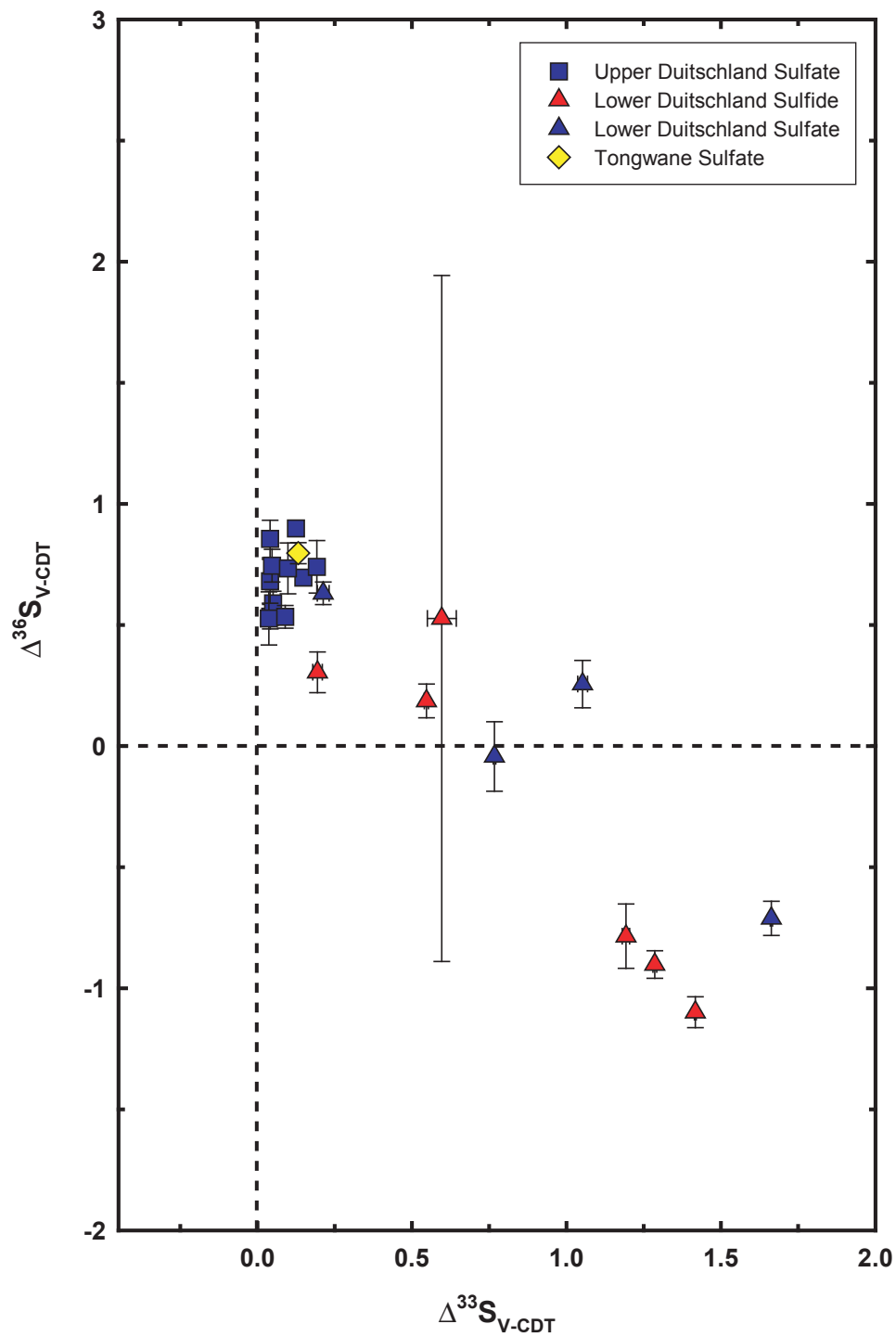
Figure 12 Isotopic plot of $\Delta^{36}S$ values against $\Delta^{33}S$ values for all samples from this study that define an array $\Delta^{33}S/\Delta^{36}S \approx -0.9$, similar to that found by Farquhar *et al.* (2000) and Farquhar *et al.* (2001).

sample has a $\Delta^{33}S$ value of +0.13 and a $\Delta^{36}S$ value of +0.8. The Duitschland Formation samples have $\Delta^{33}S$ and $\Delta^{36}S$ values ranging from +0.05 to +1.42 and -1.1 to +0.9, respectively. Figure 12 shows a plot of $\Delta^{33}S$ and $\Delta^{36}S$ values for this study's samples that define an array $\Delta^{33}S/\Delta^{36}S \approx$ -0.9, similar to that found by Farquhar *et al.* (2000) and Farquhar *et al.* (2001).

4.2.0 Carbon and Oxygen Isotopic Data

4.2.1 $\delta^{13}C_{carb}$ Isotopic Data

The carbonate samples from the study were analyzed for carbon and oxygen isotopic compositions. Figure 13 shows the carbonate $\delta^{13}C$ values for samples from this study and samples from the Bekker *et al.* (2001) study of the Duitschland Formation compared to the stratigraphic position of each sample. The two studies show good correlation. The carbon isotopic data also suggests a difference for samples above and below the interval defined by DF05-P and DF19-C. Carbon isotopic values for samples below DF05-P (n=5) are primarily negative, ranging from -1.71 to -0.3, with the exception of DF18-C that has a $\delta^{13}C_{carb}$ value of 0.01. This sample is less than 100m above DF17-C that has the most negative $\delta^{13}C_{carb}$ value in the lower section of the study area. The Tongwane Formation sample (TR01-C) has a $\delta^{13}C_{carb}$ value of -0.56, similar to the other samples from this lower section of the study area. Samples above DF05-P (n=11) are positive, ranging from +1.62 to +7.81. Samples surrounding the upper diamictite in the Duitschland Formation – DF14-C, DF13-C and DF10-C – are marked by
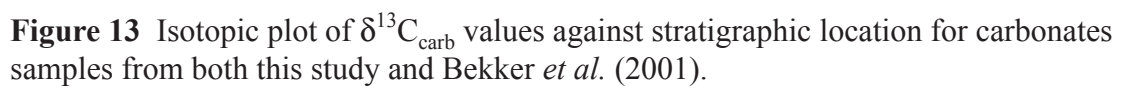
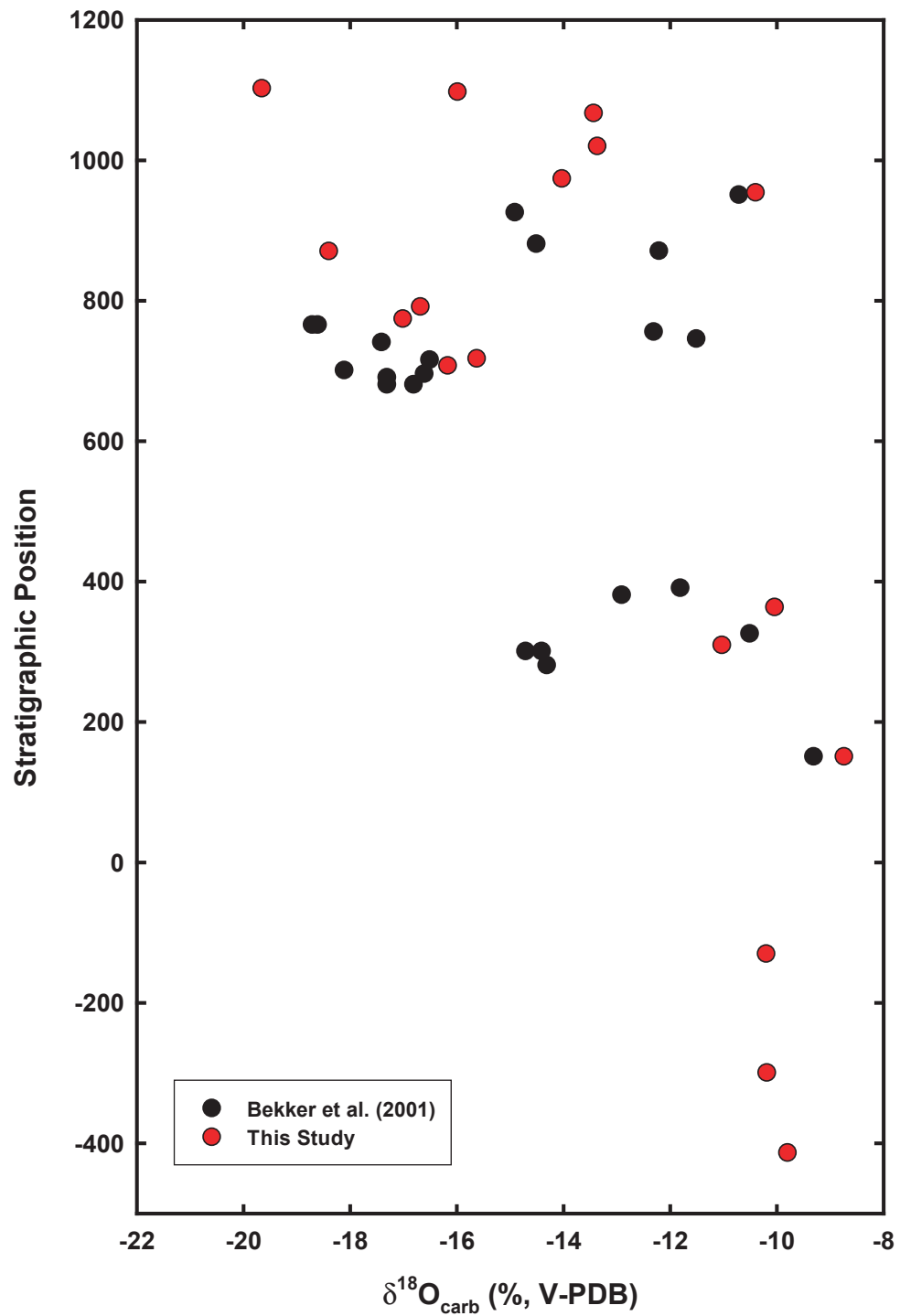a decrease in $\delta^{13}C_{carb}$ compared to the other samples in the upper portion of the study area.

4.2.2 $\delta^{18}O_{carb}$ Isotopic Data

Figure 14 shows the oxygen isotopic data for carbonates from this study compared to samples from Bekker *et al.* (2001). The $\delta^{18}O_{carb}$ values from this study record a slight trend with less negative values in samples from the Malmani Subgroup, the Penge BIF, and the lower Duitschland Formation and more negatives values from samples in the upper Duitschland Formation. The Tongwane Formation sample (TR01-C) has a $\delta^{10}O_{carb}$ value of -8.73, which is within the range of values for the lower samples (-11.02 to -9.79). Samples from the upper Duitschland Formation have a range of $\delta^{18}O_{carb}$ values from -19.64 to -10.39.

4.3 Comparison of Sulfur and Carbon Isotopic Data

The trends of the $\delta^{34}S$ values and the $\delta^{13}C$ values show a similar variation with samples below DF05-P having lower values than those samples above DF19-C (Fig. 10) as described in the previous sections. Figure 15 shows $\delta^{13}C_{carb}$ values compared to $\delta^{34}S$ values for the carbonate samples from the study area. Samples from the Malmani Subgroup, the Tongwane Formation, and the lower portion of the Duitschland Formation have lower $\delta^{34}S$ and $\delta^{13}C$ values than samples from the upper section of the Duitschland Formation. They show a small range in $\delta^{13}C$ values (~2‰) and cover a range of ~15‰ in

Figure 13 Isotopic plot of $\delta^{13}C_{carb}$ values against stratigraphic location for carbonates samples from both this study and Bekker *et al.* (2001).

Figure 14 Plot of $\delta^{18}O_{carb}$ values for carbonate samples from this study adn Bekker *et al*. (2001). The highly negative oxygen isotopic values suggest that these rocks have been influenced by hot fluids.

$\delta^{34}S$ values. The Tongwane Formation sample (TR01-C) is characterized by a $\delta^{13}C$ value similar to the other lower samples; however, the $\delta^{34}S$ value from this sample is more in line with the values of samples from the upper Duitschland Formation. Samples from the upper Duitschland Formation define a region of positive $\delta^{34}S$ and $\delta^{13}C$ values.

Figure 16 shows $\delta^{13}C$ compared to $\Delta^{33}S$ values for carbonates from this study. Again the data falls into two distinct groupings, with samples below DF05-P recording high variability in the $\Delta^{33}S$ values and low variability in the $\delta^{13}C$ values. Two of these lower portion samples – DF18-C and TR01-C – have $\Delta^{33}S$ values more in line with values for samples from the upper Duitschland Formation; however, the $\delta^{13}C$ values for these samples are close to zero. Samples from the upper Duitschland Formation have restricted $\Delta^{33}S$ values and a ~6‰ range in $\delta^{13}C$ values.
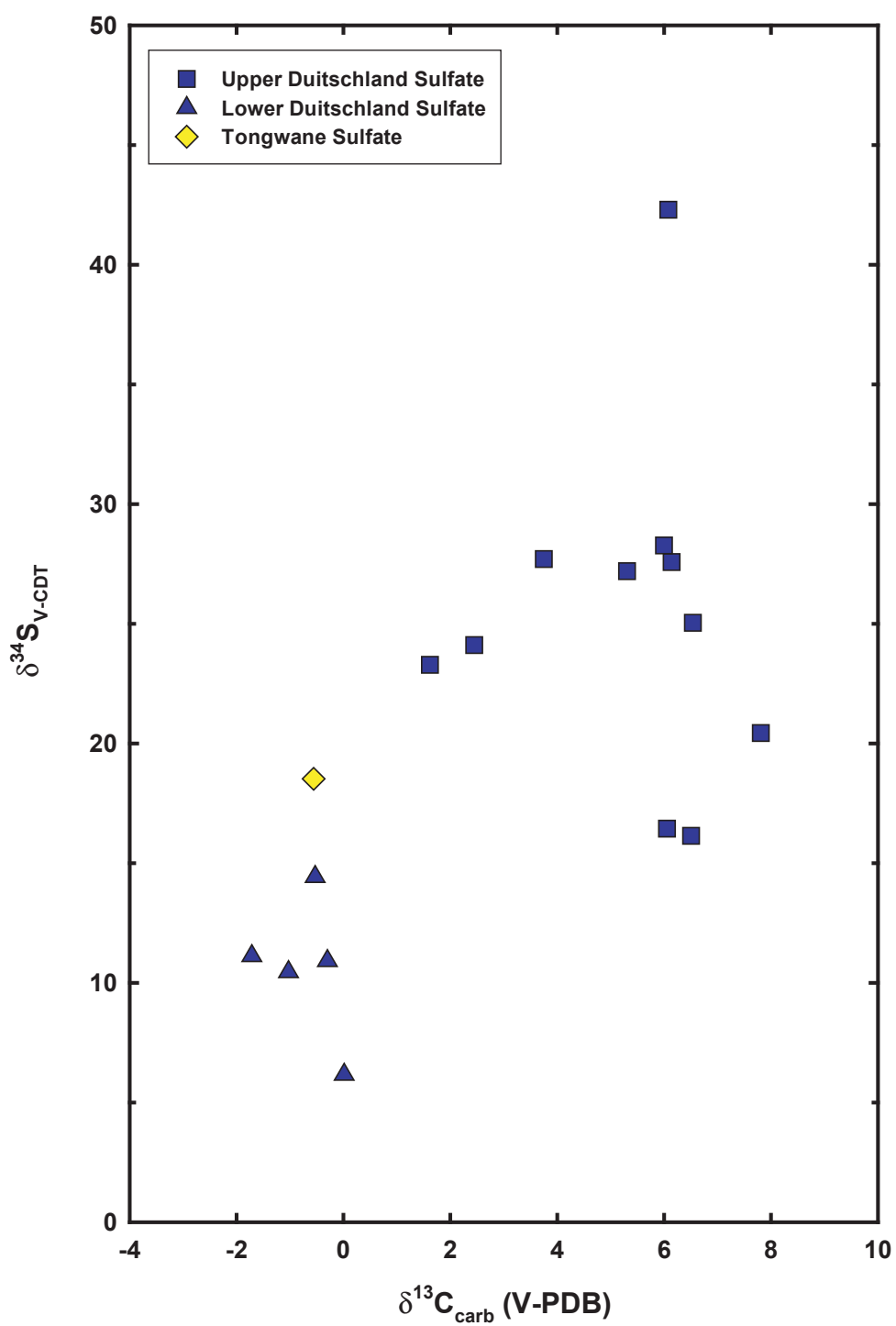
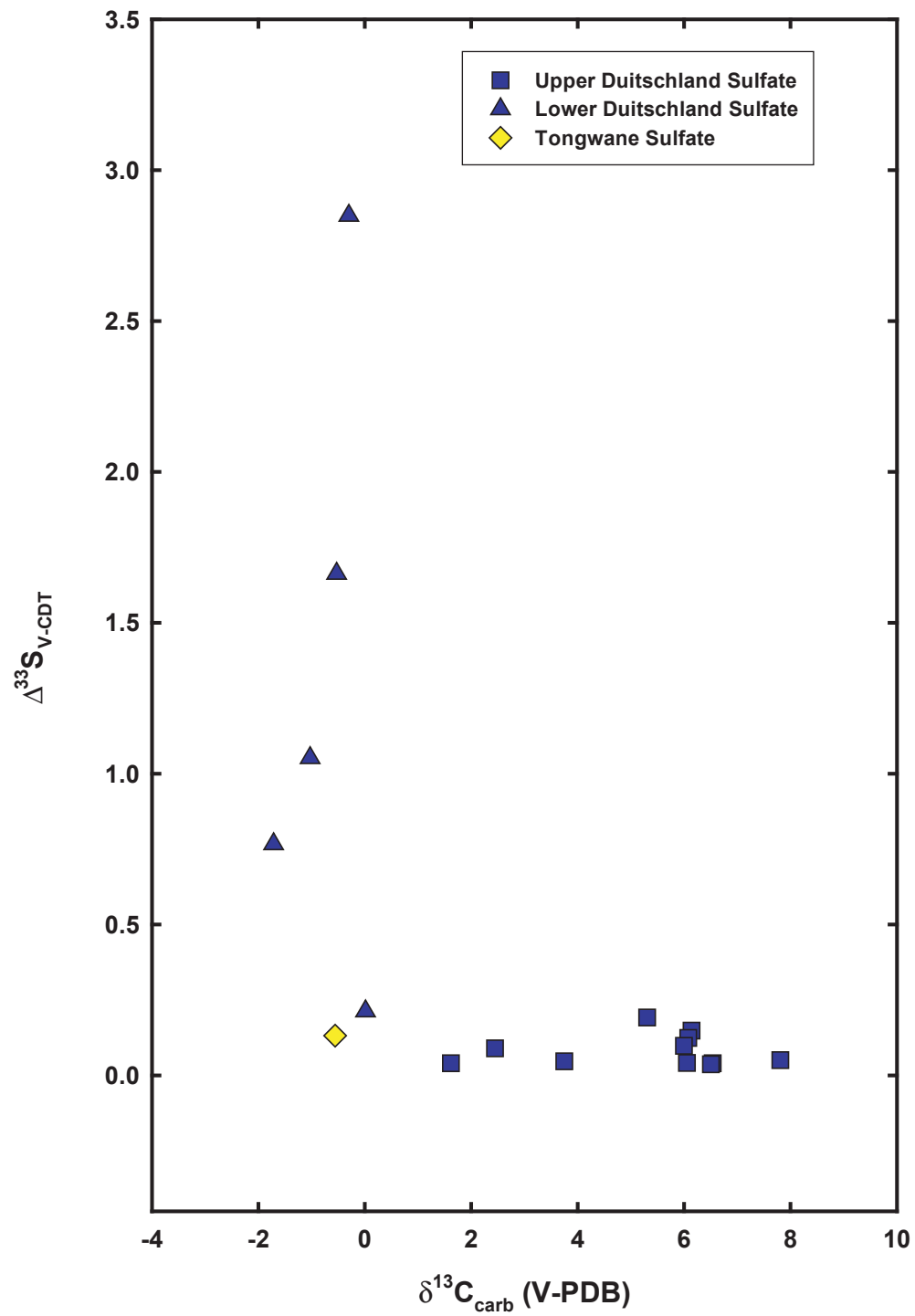**Figure 15** Isotopic plot of $\delta^{13}C$ values against $\delta^{34}S$ values for all carbonate samples from this study.

Figure 16 Isotopic plot of $\delta^{13}C$ values against $\Delta^{33}S$ values for all carbonate samples from this study.

5.0 Discussion

5.1 Preservation of Isotopic Trends in Duitschland Farm Samples

The stratigraphy of the study area is in agreement with the stratigraphy published in Bekker *et al.* (2001) and Coetzee (2001) for the Duitschland Farm of the Duitschland Formation. The study area progresses from carbonates in the Malmani Subgroup, to an ironstone in the Penge Banded Ironstone Formation (BIF), to a marly shale dominated lower Duitschland Formation that is capped with an erosional sequence boundary that is overlain by a carbonate-dominated upper Duitschland Formation. Figures 13 and 14 show the carbon and oxygen isotopic compositions, respectively, from samples collected at Duitschland Farm compared to the isotopic values from Bekker *et al.* (2001). Samples from this study are well within calculated error for the stratigraphic position based on the stratigraphic column from the published paper (Bekker *et al.*, 2001).

Similar to the Bekker *et al.* (2001) paper, this study found that the oxygen isotopic values are all highly negative ($\delta^{18}O_{carb} > -10‰$) and show a general correlation between $\delta^{18}O_{carb}$ values and stratigraphic position, with the samples from the upper Duitschland Formation recording more negative values than those from the Malmani Subgroup and the lower Duitschland Formation. These highly negative $\delta^{18}O_{carb}$ values suggest that these rocks have been influenced by hot fluids associated with intrusion of mafic sills associated with the intrusion of the Bushveld Complex to the northwest of the study location.

The effects of metamorphic fluid-flow, however, do not invalidate the carbon isotopic data from this study. Figure 17 shows a plot of $\delta^{13}C_{carb}$ versus $\delta^{18}O_{carb}$ for

63

carbonates from the study area that shows no correlation between these isotopic values.

Several studies have shown that despite some degree of chemical alteration during

digenetic processes and low-grade metamorphism, the $\delta^{13}C$ composition of Archean and

Paleoproterozoic carbonates is relatively unaffected by chemical overprinting from these

processes. The high concentration of carbon in the carbonates compared to the relatively

low concentration in any digenetic or metamorphic fluid leads to a more resistant $\delta^{13}C$

composition than that of $\delta^{18}O$ (Ferry, 1994; Halverson *et al.*, 2005).

5.2.0 Sulfur Isotopic Analysis

5.2.1 $\delta^{34}S$ Isotopic Data

Within the general increase in $\delta^{34}S$ values in the study area, there are oscillations

that appear to be connected to changes in sea level and glacial events. Samples from the

Malmani Formation show a slight increase then a slight decrease from the base to the

overlying Penge Banded Ironstone Formation (BIF). On Duitschland Farm, there is a

glacial diamictite directly above the Penge BIF. The Tongwane Formation, which lies

between the Penge BIF and the glacial-based Duitschland Formation, records a sizeable

increase in the $\delta^{34}S$ values that may be related to its clastic nature, suggesting that there

was increased weathering of silicate materials during this interval. Increased weathering

of continental material could have led to enhanced biological activity in the

Paleoproterozoic ocean. Above the glacial diamictite (Fig. 10), the $\delta^{34}S$ values gradually
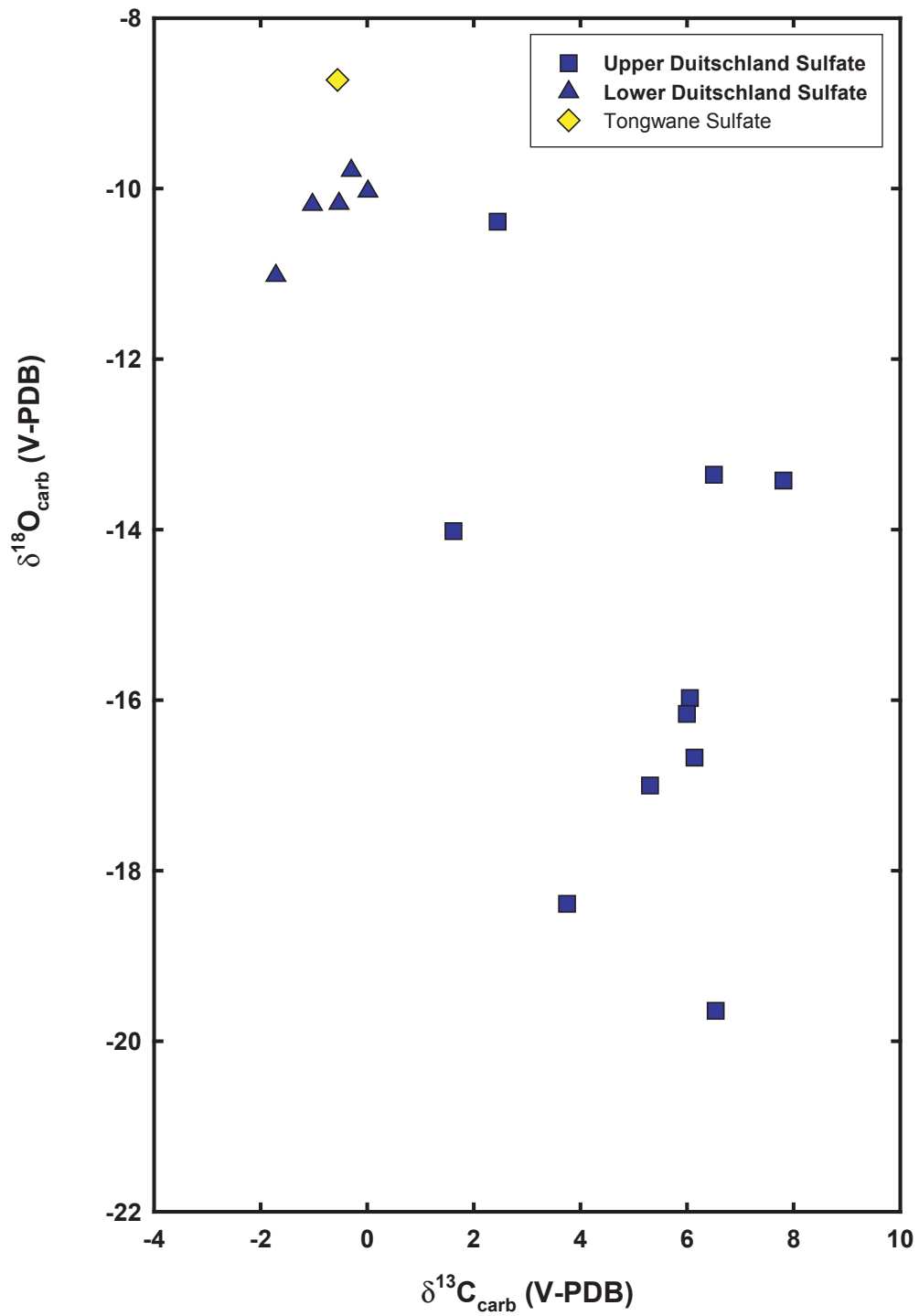
decrease to levels close

Figure 17 Plot of oxygen and carbon isotopic values for carbonate samples from the study area. The highly negative oxygen isotopic values suggest that these rocks have been influenced by hot fluids.

to zero until the sequence boundary quartzite. Comparing the range of sulfate and sulfide

values in this lower section show that the fractionation between these two reservoirs was

low. Above the last sulfide sample, the δ^{34}S values jump from close to zero to around

+30‰.

5.2.2 Δ^{33}S Isotopic Data

The Δ^{33}S values for the study area show an overall decrease, with the highest

values at the base of the succession and close to zero values in the upper portion of the

Duitschland Formation (Fig. 10). Within this broader trend, there are several smaller

trends including the systematic increase from the Malmani Formation through the Penge

BIF and the Tongwane Formation. While it is tempting to draw a direct connection

between the Δ^{33}S values and the amount of free atmospheric oxygen, there is no evidence

to directly link an increasing Δ^{33}S trend to a gradual build up of atmospheric oxygen. It

is possible, however, that future research will provide a method in which Δ^{33}S values

could provide a quantity of O_2 available at the time of deposition. Despite this inability

to qualify the amount of O_2 present during the time of the Duitschland Formation and the

Malmani Subgroup, it is likely that the variations recorded by the sulfide samples above

and below the sequence boundary reflect a change in the concentration of atmospheric

O_2. The close to zero values for sulfate samples above the sequence boundary are

consistent with an atmosphere containing oxygen concentrations great than 10^{-5} present

atmospheric levels (PAL).

5.2.3 $\delta^{13}C_{carb}$ Isotopic Data

The $\delta^{13}C_{carb}$ values for samples from the Duitschland Formation show a similar range values as those reported by Bekker *et al.* (2001), with values close to zero in the lower portion and highly positive values at the top of the formation. Isotopic values from this study shows that the samples from the Malmani Subgroup, Tongwane Formation, and lower portion of the Duitschland Formation have little variability (Fig. 10). There is a slight $\delta^{13}C$ increase in values in the lower Duitschland Formation directly below the sequence boundary. This increase, however, is small in comparison to the increase in the $\delta^{13}C_{carb}$ values for samples from the upper Duitschland Formation. In this upper portion, there is a systematic decrease from the lowest sample to directly below the upper diamictite that was identified by Bekker *et al.* (2001). The $\delta^{13}C_{carb}$ values of the four upper-most samples return to values similar to those prior to this glacial event.

5.3 Paleoenvironmental Interpretations

Isotopic evidence from the Duitschland Formation suggests a critical transition of the surface environment at the time of the deposition of the Malmani Supergroup, the Penge BIF and Duitschland formations. Individually, the isotopic data presented here supply information on aspects of the paleoenvironment. Minor sulfur isotopic ($\Delta^{33}S_{V\text{-}CDT}$) data record the build of up free oxygen in the atmosphere to a threshold level of 10^{-5} PAL (Farquhar *et al.*, 2000; Farquhar *et al.*, 2002; Farquhar & Wing, 2003). Carbon isotopic ($\delta^{13}C_{carb}$) data from carbonate samples provide information on the flux of relative organic matter to carbonate matter in the paleoenvironment. This flux is related to the

availability of nutrients in the oceanic environment as well as rates of biological activity. Variations provide information about oceanic sulfate chemistry, namely prior workers have argued that fractionation for $\delta^{34}S$ between sulfate and elemental sulfur is greater than 20‰ reflect sulfate concentrations of greater than 200 micromole. The $\delta^{34}S$ values for CAS from sample in the upper Duitschland Formation are 20-30‰ and are consistent with these finding. The $\delta^{34}S$ values of samples at the sequence boundary are ~5-20‰ and the CAS is also greater than 20‰ below the sequence boundary, suggesting that the concentration of oceanic sulfate was less than 200 micromolar. When these data are reviewed together with lithological evidence of climate changes, a more complex picture of sulfur and carbon cycling during the critical biogeochemical transitions that occurred between 2480 and 2316 Ma can be constructed.

The carbon isotopic data from this study and those published by Bekker *et al.* (2001) for carbonates in the Malmani Subgroup and the lower Duitschland Formation have near zero or negative $\delta^{13}C$ values (+0.01 to -1.71 ‰), and carbonate samples from the upper Duitschland Formation are enriched in ^{13}C with a maximum $\delta^{13}C$ value of +7.81‰. The upper formation samples show a general trend towards lower $\delta^{13}C_{carb}$ values that then return to higher $\delta^{13}C_{carb}$ values at the very top of the Duitschland Formation. This general trend of near zero levels in the lower Duitschland Formation to elevated $\delta^{13}C$ values in the upper Duitschland Formation suggest the enhanced proportional burial of organic carbon most likely due to increased biological activity. The climate at the time of the deposition of the upper Duitschland Formation was doubtlessly warmer than the glacial environment recorded in the diamictite at the base of the formation. Biological activity is inferred to have been enhanced in the warmer

climate by an increase in the delivery of nutrients to the oceans due to intensifying silicate weathering immediately following this glacial event.
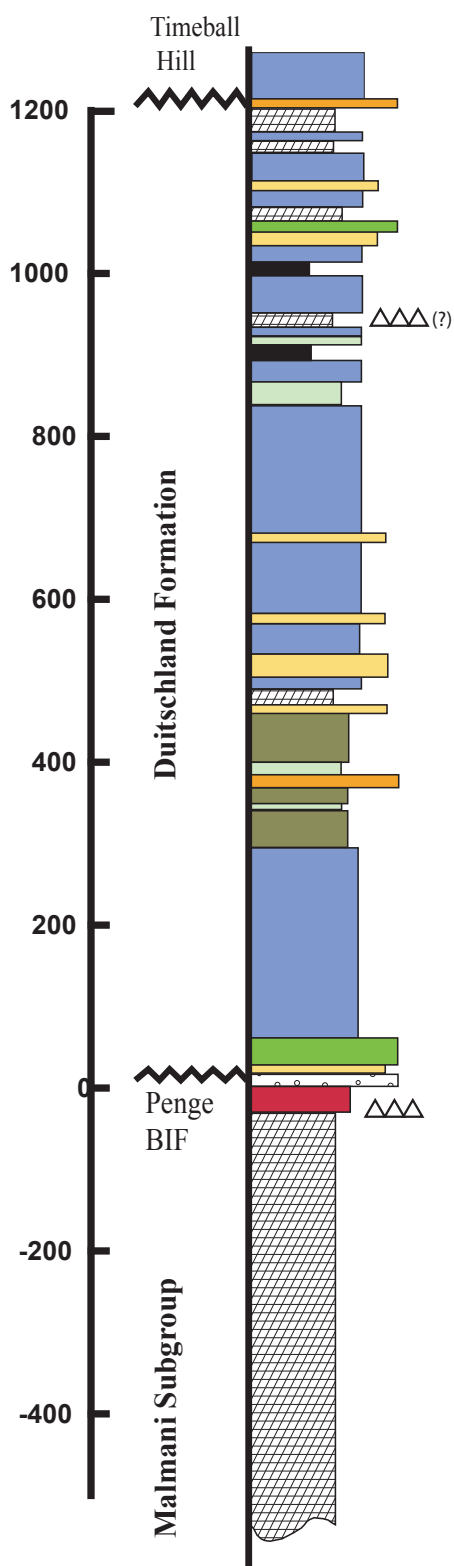
The minor sulfur isotopic trend shows that samples in the lower Duitschland Formation and underlying Penge BIF and Malmani Subgroup have variable $\Delta^{33}S$ values (+0.213 to +1.417‰); whereas, samples from the upper Duitschland Formation have limited $\Delta^{33}S$ values (+0.037 to +0.192‰). Samples from the lower Duitschland Formation and below include sulfur isotopic compositions with mass-independent fractionation values ($\Delta^{33}S > \pm0.5$‰).

Recorded in the study area is the transition from a surface environment with limited free atmospheric oxygen to an oxic environment. This transition indicates, according to the Pavlov and Kasting (2002) calculations, that the partial pressure of atmospheric oxygen exceeded the threshold level (10^{-5} PAL) above which the mass independent fractionation signal is not transferred effectively to the rock record. This trend is supported by the $\Delta^{36}S$ values for the study area. Farquhar *et al.* (2000) note that there is a negative relationship between $\Delta^{33}S$ and $\Delta^{36}S$ values since an environment with limited free oxygen and no ozone layer will allow deep ultraviolet radiation to penetrate through the entire atmosphere and to the Earth's surface to produce mass-independent fractionation signals in both minor sulfur isotopes. Samples from the lower Duitschland Formation and below have a negative correlation; whereas, there is no linear correlation between these isotopic values for samples from the upper Duitschland Formation.

The major sulfur isotopic trend suggests that there was a fundamental shift in the ocean sulfate concentration and biological cycling of sulfur, which is supported by the carbon isotopic data. Work by Habicht *et al.* (2002) indicates that the fractionation of
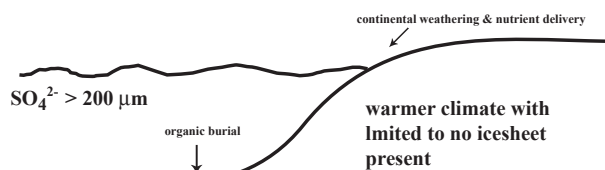
sulfur by sulfate-reducing bacteria will be suppressed at oceanic sulfate concentrations below 200 μM. The small fractionation (~10‰) between coeval sulfate and sulfide from samples in the lower Duitschland Formation and below suggest that the oceanic sulfate concentration was less than 200 μM at the time of deposition. There are no sulfide samples from the upper Duitschland Formation, however, sulfide samples from the lower Timeball Hill Formation (Bekker et al., 2004) are a close approximation of coeval sulfide samples for the upper section of this study. The large fractionation (~45‰) between coeval sulfate and sulfide samples indicate the oceanic sulfate levels were above 200 μM at the time of deposition.

Taken together these isotopic data indicate that there was a critical transition in the carbon and oxygen cycles as well as a fundamental change in the biological activity (Fig. 18). The paleoenvironment during this interlude can be divided generally into two stages: prior to the rise of atmospheric oxygen above the threshold 10^{-5} PAL level (Stage 1) and subsequent to the rise of atmospheric oxygen above this level (Stage 2). Prior to the deposition of the Penge BIF (Stage $1A_1$), the paleoenvironment was warm enough to support an ice-free environment where the oceans had limited sulfate levels and biological activity was relatively low. The atmospheric oxygen levels were sufficiently low enough to record $\Delta^{33}S$ values consistent with mass-independent fractionation. This stage was terminated by the deposition of the Penge BIF, a period of cooler climate as recorded by the glacial diamictite at the base of the Duitschland Formation. The next stage of environmental evolution (Stage $1A_2$) occurred after the melting of the glacial event and prior to the development of the erosional sequence boundary at ~ 400 m above the basal contact with the Penge BIF. Atmospheric oxygen levels increased from lower
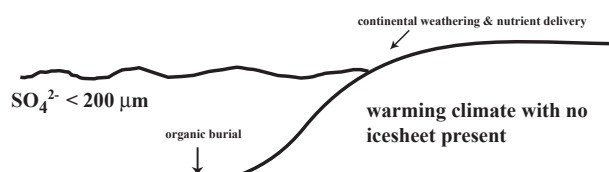
Timeball
Hill

1200

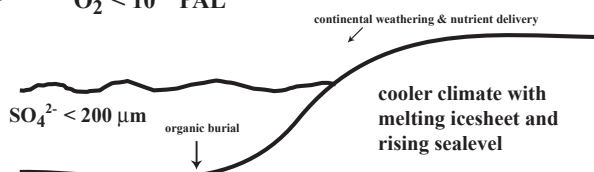Duitschland Formation

1000

800

600

400

200

0

Penge
BIF

Malmani Subgroup

-200

-400

2

$O_2 > 10^{-5}$ PAL

continental weathering & nutrient delivery

$SO_4^{2-} > 200$ μm

organic burial

warmer climate with
lmited to no icesheet
present

1B

$O_2 < 10^{-5}$ PAL

continental weathering & nutrient delivery

$SO_4^{2-} < 200$ μm

organic burial

warming climate with no
icesheet present

1A$_2$

$O_2 < 10^{-5}$ PAL

continental weathering & nutrient delivery

$SO_4^{2-} < 200$ μm

organic burial

cooler climate with
melting icesheet and
rising sealevel

1A$_1$

$O_2 < 10^{-5}$ PAL

continental weathering & nutrient delivery

$SO_4^{2-} < 200$ μm

organic burial

cooler climate with
growing icesheet and
lowering sealevel

(?)

values to those similar to the level of free oxygen prior to the deposition of the Penge BIF. At this time there was a slight increase in biological activity in a sulfate-limited ocean. The termination of this stage is marked by the erosional surface of the sequence boundary, suggesting a lowering of sea level or the exposure of this region to surficial weathering processes. There is an interval (Stage 1B) after the sequence boundary wherein the atmospheric oxygen levels changed relatively rapidly, in comparison to the two previous rises in atmospheric free oxygen, to levels above 10^{-5} PAL. During this time, the biological activity and oceanic chemistry was near identical to the environment prior to the sequence boundary.

The last interval (Stage 2) records an ice-free environment in which the atmospheric oxygen is above 10^{-5} PAL. Biological activity is high due in part to the increased delivery of nutrients from the continents to the oceans as a result of increased silicate weathering, which in turn could increase the sulfate budget in the oceans. Samples from the upper Duitschland Formation record low variability in $\Delta^{33}S$ values, suggesting an oxic surface environment, and a wide variability in $\delta^{34}S$ values, indicating an oceanic sulfate concentration similar to today's value. The $\delta^{13}C_{carb}$ values for these samples indicate that there was an increase in the burial of organic material and an increased influence by photosynthetic biological activity. In the upper Duitschland Formation, the paleoenvironment changed so that there was an increase in the oceanic sulfate concentration that coincides with the rise of atmospheric oxygen due in part to the increased silicate weathering of continental materials. The previous balance of biological

---

Figure 18 Schematic diagram of the inferred paleoenvironment for the northern Transvaal Basin between 2.3-2.4 Ga during the reorganization of the sulfur and carbon cycles due to changes in climate and biological activities. The stages noted in the upper left corner of each box correspond to those discussed in the text. Length and size of arrows indicate the intensity of the flux.

activity and oxidation of reduced sulfur and carbon species was overtaken by a large increase in biological activity in response to a new influx of nutrients from continental weathering.

Taken together, the sulfur isotopic data and carbon isotopic data presents a fundamental reorganization of the sulfur and carbon cycles as well as a transition in the biological activity of the oceans during the *ca.*165 million years of deposition of the Duitschland Formation. The sulfur cycle in the lower portion of the study area is dominated by photochemical processes with limited biological input. Once the surface environment transitioned to oxic, the sulfur cycle reorganized to a system very similar to the modern sulfur cycle that is dominated (in the short-term) by biological fractionation.

6.0 Overview of Findings

- The rise of atmospheric oxygen is recorded in the Duitschland Formation from the Transvaal Basin, South Africa.

- The $\Delta^{33}S$ values record the rise of atmospheric oxygen from a level below the calculated 10^{-5} present atmospheric level (PAL; Pavlov & Kasting, 2002) to above this threshold for recording mass-independent fractionation signals in the rock record.

    - Samples from the lower Duitschland Formation and below were deposited in an anoxic surface environment.

    - Samples from the upper Duitschland Formation were deposited in an oxic surface environment.

- The $\delta^{34}S$ data suggests that the ocean sulfate concentration increased from less than 200 μM based on the coeval sulfate-sulfide pairs to a greater concentration.

- The $\delta^{13}C_{carb}$ data record an increased proportional burial of organic carbon in the upper Duitschland Formation.

References

Aharon, P. (2005). Redox stratification and anoxia of the early Precambrian oceans: Implications for carbon isotope excursions and oxidation events. *Precambrian Research* 137, pp. 207-222.

Bains-Sahota, S.K. and Thiements, M.H. (1989). A mass-independent sulfur isotope effect in the nonthermal formation of S_2F_{10}. *Journal of Chemical Physics* 90, pp. 6099-6109.

Bekker, A., Kaufman, A.J., Karhu, J.A., Beukes, N.J., Swart, Q.D., Coetzee, L.L., & Eriksson, K.A. (2001). Chemostratigraphy of the Paleoproterozoic Duitschland Formation, South Africa: Implications for coupled climate change and carbon cycling. *American Journal of Science* 301, pp. 261-285.

Bekker, A., Holland, H.D., Wang, P.-L., Rumble III, D., Stein, H.J., Hannah, J.L., Coetzee, L.L., & Beukes, H.J., (2004). Dating the rise of atmospheric oxygen. *Nature* 427, pp. 117-120.

Burdett, J.W., Arthur, M.A., & Richardson, M. (1989). A Neogene seawater sulfur isotope age curve from calcareous palegic microfossils. *Earth and Planetary Science Letter* 94, pp. 189-198.

Canfield, D.E. (2005). The Early History of Atmospheric Oxygen: Homage to Robert M. Garrels. *Annual Reviews of Earth and Planetary Sciences* 33, pp. 1-36.

Catling, D.C. and Claire, M.W. (2005). How Earth's atmosphere evolved to an oxic state: A status report. *Earth and Planetary Science Letter Frontiers*

Catling, D.C., Zahnle, K.J., and McKay, C.P. (2001). Biogenic methane, hydrogen escape, and the irreversible oxidation of early Earth. *Science* 293, pp. 839-843.

Cloud, P.E. (1972). A working model of the primitive Earth. *American Journal of Science* 272, pp. 537-548.

Cloud, P. E. (1988). Oasis in Space, Earth History from the Beginning: New York, W. W. Norton, p. 508.

Coetzee, L. L.. *Genetic Stratigraphy of the Paleoproterozoic Pretoria Group in the Western Transvaal* Thesis, Rand Afrikaans Univ. (2001).

Des Marais, D.J. (2001). Isotopic Evolution of the Biogeochemical Carbon Cycle During the Precambrian. *In* Stable Isotope Geochemistry. J.W. Valley and D.R. Cole (Eds.). Mineralogical Society of America, Washington, DC, pp. 555-578.

Ding T., Valkiers, S., Kipphardt, H., De Bievre, P., Taylor, P.D.P., Gonfiantini, R., and Krouse R. (2001). Calibrated sulfur isotope abundance ratios of three IAEA sulfur isotope reference materials and V-CDT with a reassessment of the atomic weight of sulfur. *Geochimica et Cosmochimica Acta* 65, pp. 2433-2437.

Eriksson, P.G., Schweitzer, J.K., Bosch, P.J.A., Schereiber, U.M., Van Deventer J.L., & Hatton, C.J. (1993). The Transvaal Sequence: an overview. *Journal of African Earth Sciences* 16 (1/2), pp. 25-51.

Eriksson, P.G., Altermann, W., Catuneanu, O., ven der Merwe, R., & Bumby, A.J. (2001). Major influences on the evolution of the 2.67-2.1 Ga Transvaal basin, Kaapvaal craton. *Sedimentary Geology* 141-142, pp. 205-231.

Farquhar, J., Bao, H., & Thiemens, M. (2000). Atmospheric Influence of Earth's Earliest Sulfur Cycle. *Science* 289, pp. 756-758.

Farquhar, J., Wing, B.A., McKeegan, K.D., Harris, J.W., Cartigny, P. & Thiemens, M.H. (2002). Mass-Independent Sulfur of Inclusions in Diamond and Sulfur Recycling on Early Earth. *Science* 298, pp. 2369-2372.

Farquhar, J. and Wing, B.A., (2003). Multiple sulfur isotopes and the evolution of the atmosphere. *Earth and Planetary Science Letters* 213, pp. 1-13.

Ferry, J.M. (1994). Role of fluid flow on contact metamorphism of siliceous dolomitic limestone. *American Mineralogist* 79, pp. 719-736.

Forrest, J. and Newman, L. (1977). Silver-110 Microgram Sulfate Analysis for the Short Time Resolution of Ambient Levels of Sulfur Aerosol. *Analytical Chemistry* 49 (11), pp. 1579-1584.

Habicht, K.S., Gade, M., Thamdrup, B., Berg, P., & Canfield, D.E. (2002). Calibration of Sulfate Levels in the Archean Ocean. *Science* 298, pp. 2372-2374.

Hannah, J.L., Bekker, A., Stein, H.J., Markey, R.J., & Holland, H.D. (2004). Primitive Os and 2316 Ma age for marine shale: implications for Paleoproterozoic glacial events and the rise of atmospheric oxygen. *Earth and Planetary Science Letters* 225, pp. 43-52.

Halverson, G.P., Hoffman, P.F., Schrag, D.P., Maloof, A.C., and Rice, A.H.N. (2005). Toward a Neoproterozoic composite carbon-isotope record. *GSA Bulletin* 117, pp. 1181-1207.

Hayes, J.M., Strauss, H., and Kaufman, A.J. (1999). The abundance of ^{13}C in marine organic matter and isotopic fractionation in the global biogeochemical cycle of carbon during the past 800 Ma. *Chemical Geology* 161, pp. 103-125.

Hulston, J.R. and Thode, H.G. (1965). Cosmic-Ray-Produced S36 and S33 in Metallic Phase of Iron Meteorites. *Journal of Geophysical Research* 70 (18), pp. 4435.

Hsieh, Y.P. and Shieh, Y.N. (1997). Analysis of reduced inorganic sulfur by diffusion methods: improved apparatus and evaluation of sulfur isotopic studies. *Chemical Geology* 137, pp. 255-261.

Hu, G., Rumble, D., and Wang, P.L. (2003). An ultraviolet laser microprobe for the in situ analysis of multisulfur isotopes and its use in measuring Archean sulfur isotope mass-independent anomalies. *Geochimica et Cosmochimica Acta* 67, pp. 3101-3117.

Karhu, J.A. and Holland, H.D. (1996). Carbon isotopes and the rise of atmospheric oxygen. *Geology* 24, pp.867-870.

Kasting, J.F. (1993). Earth's Early Atmosphere. *Science* 259, pp. 920-926.

Kasting, J.F. (2001). The Rise of Atmospheric Oxygen. *Science* 293, pp. 819-820.

Kasting, J.F. (2005). Methane and climate during the Precambrian era. *Precambrian Research* 137, pp. 119-129.

Kasting, J.F. and Catling, D. (2003). Evolution of a Habitable Planet. *Annual Reviews of Astronomy and Astrophysics* 41, pp. 429-463.

Kerr, R.A. (2005). The story of O_2. *Science* 308, pp. 1730-1732.

Kump, L.R. and Arthur, A.A. (1999). Interpreting carbon-isotope excursions: carbonates and organic matter. *Chemical Geology* 161, pp. 181-198.

Machel, H.G. and Burton, E.A. (1991). Factors governing cathodoluminescence in calcite and dolomite, and their implications for studies of carbonate diagenesis. *In* LuminescenceMicroscopy: Quantitative and Qualitative Aspects. C.E. Barker and O.C. Kopp (Eds.). SEPM, pp. 37-57.

Machel, H.G., Mason, R.A., Mariano, A.N., and Mucci, A. (1991). Causes and emission of luminescence in calcite and dolomite. *In* LuminescenceMicroscopy: Quantitative and Qualitative Aspects. C.E. Barker and O.C. Kopp (Eds.). SEPM, pp. 9-25.

Melezhik, V.A., Fallick A. E., Hanski, E.J., Kump, L.R., Leplan, A., Prave, A.R., and Strauss, H. (2005). Emergence of the aerobic biosphere during the Archean-Proterozoic transition: Challenges of future research. *GSA Today* 15, pp.4-11.

Mojzsis, S.J., Coath, C.D., Greenwood, J.P., McKeegan, K.D., & Harrison, T.M. (2003). Mass-independent isotope effects in Archean (2.5 to 3.8 Ga) sedimentary sulfides determined by ion microprobe analysis. *Geochimica et Cosmochimica Acta* 67 (9), pp. 1635-1658.

Nelson, D.R., Trendall, A.F., and Altermann, W. (1999). Chronological correlation between the Pilbara and Kaapvaal cratons. *Precambrian Research* 97, pp. 165-189.

Nisbet, E.G. and Sleep, N.H. (2001). The habitat and nature of early life. *Nature* 409, pp. 1083-1091.

Ono, S., Eigenbrode, J.L., Pavlov, A.A., Kharecha, P., Rumble, III, D., Kasting, J.F. & Freeman, K.H. (2003). New insights into the Archean sulfur cycle from mass-independent sulfur isotope records from the Hamersley Basin, Australia. *Earth and Planetary Science Letters* 213, pp. 15-30.

Pavlov, A.A. and Kasting, J.F. (2002). Mass-Independent Fractionation of Sulfur Isotopes in Archean Sediments: Strong Evidence for an Anoxic Archean Atmosphere. *Astrobiology* 2 (1), pp. 27-41.

Ripperdan, R.L. (2001). Stratigraphic Variation in Marine Carbonate Carbon Isotope Ratios. *In* Stable Isotope Geochemistry. J.W. Valley and D.R. Cole (Eds.). Mineralogical Society of America, Washington, DC, pp. 637-662.

Rye, R. and Holland, H.D. (1998). Paleosols and the Evolution of Atmospheric Oxygen: A Critical Review. *American Journal of Science* 298, pp. 621-672.

Sumner, D.Y. and Grotzinger, J.P. (2004). Implications for Neoarchaean ocean chemistry from primary carbonate mineralogy of the Campbellrand-Malmani Platfor, South Africa. *Sedimentology* 51, pp. 1273-1299.

Tian, F., Toon, O.B., Pavlov, A.A., and De Sterck, H. (2005). A Hydrogen-rich Early Earth Atmosphere. *Science* 308, pp. 1014-1017.

Thiemens, M.H. (1999) Mass-Independent Isotope Effects in Planetary Atmospheres and the Early Solar System. *Science* 283, pp. 341-345.

Thode, H.G., Monster, J., & Dunford, H.B. (1961) Sulphur Isotope Geochemistry. *Geochimica et Cosmochimica Acta* 25, pp. 159-174.

Walker, J.C.G. (1977) Evolution of the Atmosphere. McMillan: New York.